SLAC-PUB-2402
September 1979
(T/E)

MASSIVE LEPTON PAIR PRODUCTION*

R. Stroynowski

Stanford Linear Accelerator Center
Stanford University, Stanford, California 94305

Lectures

at

the

SLAC Summer Institute on Particle Physics:

Quantum Chromodynamics

at

Stanford, California

July 9 - 20, 1979

*This work was supported by the Department of Energy under contract number DE-AC03-76SF00515.

TABLE OF CONTENTS

1. Introduction

2. The Drell-Yan Mechanism

   2.1 Definitions and Variables

   2.2 Light Cone Variables

   2.3 Subprocess Cross Section

   2.4 Differential Cross Sections

   2.5 Drell-Yan Process in QCD

3. Particle Type Dependence

   3.1 Target Dependence

   3.2 Beam Dependence

4. Mass Spectra

   4.1 pN Interactions

   4.2 πN Interactions

5. Momentum Spectra of Lepton Pairs

   5.1 Longitudinal Momentum Distributions

   5.2 Transverse Momentum Distributions

6. QCD Phenomenology of Lepton Pair Production

7. Angular Distributions

8. Structure Functions and Quark Distributions

   8.1 Parton Model

   8.2 Quark Structure Functions

   8.3 Pion Structure Function

9. Outlook

1. INTRODUCTION

The study of high mass lepton pair production originated as a by-product of the search for new particles. In 1969, the Columbia-BNL group searching for the intermediate vector boson observed [1] the production of direct $\mu^+\mu^-$ pairs with masses of up to about 5 GeV which could not have been explained by experimental background. An explanation of the production process was proposed in 1970 by Drell and Yan [2] in terms of the quark parton model. Their approach has been, in general, successful, and it is now customary to call production of massive lepton pairs the Drell-Yan process. Today the lepton pair continuum is no more an unwanted background masking the production of resonances. It is a topical subject providing the sensitive testing ground for the various models of strong interaction dynamics. In the parton model, and recently in Quantum Chromodynamics (QCD), one can calculate a number of predictions for this process which can be tested with high accuracy.

In the first part of these lectures I will define the Drell-Yan mechanism in terms of the parton model and describe the modification expected from QCD description of the process. In Sections 3 to 5 I will review the present status of the data concentrating on the topics relevant to tests of the theory and in Sections 6 to 8 I will summarize the problems of the phenomenology of the data. For the discussion of other aspects of lepton pair production and earlier results, the reader is referred to other reviews. [3,4]

2. THE DRELL-YAN MECHANISM

2.1 Definitions and Variables:

The model proposed by Drell and Yan [2] to describe massive lepton pair production is depicted in Figure 1. In this model a quark from one

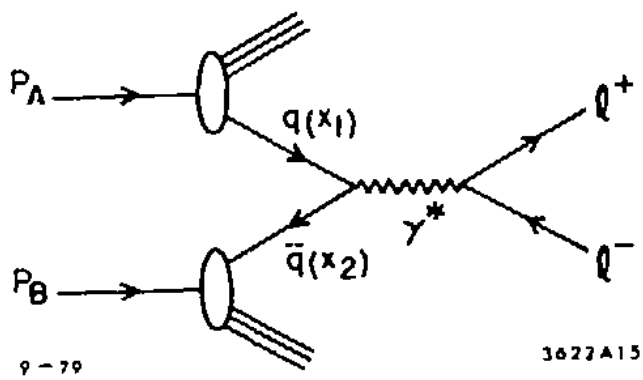

1. The Drell-Yan diagram.

of the incoming hadrons annihilates with the corresponding antiquark from the second hadron producing a virtual photon of mass M, which then decays into a pair of leptons. For simplicity one usually neglects the transverse momenta of the quarks inside the hadrons and the masses involved. The cross section is then described by:

$$\sigma = \int dx_1 dx_2 \sum_{\substack{\text{all} \\ \text{flavors}}} \left[G_{q_i/A}(x_1) G_{\bar{q}_i/B}(x_2) + G_{q_i/A}(x_1) G_{\bar{q}_i/B}(x_2) \right]$$

$$\times \sigma_i(q_i\bar{q}_i \to \gamma^*)\, \delta\left(M^2 - (k_a + k_b)^2\right) dM^2 \quad , \qquad (1)$$

where functions G(x) represent the probabilities of finding the quark or antiquark with a fraction x of the parent particle momentum.

$$k = xP$$

The variables describing the virtual photon are related to the overall center of mass energy squared s and the fractional momenta of the quarks by:

$$M^2 = (k_a + k_b)^2 = s x_1 x_2$$

$$x_F = 2 p_L / \sqrt{s} = x_1 - x_2$$

It is often convenient to introduce the scaling variable τ, $\tau = M^2/s = x_1 x_2$ representing the fraction of the total c.m. energy used in the formation of the virtual photon. The quark variables may then be expressed in terms of the lepton pair quantities by the following set of relations:

$$x_1 + x_2 = \sqrt{x_F^2 + 4\tau}$$

$$x_{1,2} = \frac{1}{2}\sqrt{x_F^2 + 4\tau} \pm x_F$$

$$x_{1,2} = \sqrt{\tau}\ e^{\pm y}$$

where y is the rapidity of the virtual photon.

2.2 Light Cone Variables:

In general the quarks may have a non-zero transverse momentum inside the parent hadrons and may be far off mass shell. In such a situation the calculation of the kinematical quantities should then be performed using light cone variables. The four vector of the incoming hadron P_A with mass M, the annihilating quark k_a, and the recoil system 1_a with mass m are then defined as follows:

$$P_A = \left(p + \frac{M^2}{4p},\ \vec{0}_\perp,\ p - \frac{M^2}{4p}\right)$$

$$k_a = \left(xp + \frac{\vec{k}_T^2 + k_a^2}{4xp},\ \vec{k}_T,\ xp - \frac{\vec{k}_T^2 + k_a^2}{4xp}\right)$$

$$1_a = \left((1-x)p + \frac{\vec{k}_T^2 + m^2}{4(1-x)p},\ -\vec{k}_T,\ (1-x)p - \frac{\vec{k}_T^2 + m^2}{4(1-x)p}\right)$$

They fulfill the energy-momentum conservation requirement:

$$k_a = P_A - 1_a$$

$$k_a^2 = x\left(M^2 - \frac{\vec{k}_T^2 + m^2}{1-x} - \frac{\vec{k}_T^2}{x}\right) .$$

Calculations using the light cone variables are usually quite complicated and in general yield results which are the same as when using the on-mass-shell kinematics. There are, however, certain regions of phase

space (e.g., the large transverse momentum region) where the use of the off-mass-shell kinematics significantly affects the results.[5]

2.3 Subprocess Cross Section:

The cross section for the subprocess of the quark-antiquark annihilation may be written in analogy to the electron-positron annihilation[6]

$$\sigma_i\left(q_i\bar{q}_i \to \gamma^*\right) = \frac{4\pi\alpha^2}{3M^2} e_i^2 \frac{1}{n}$$

where α is the electromagnetic coupling constant, e_i represents the quark charge and n is the number of colours. Since the factor $1/n$ is the same for all the $q\bar{q}$ annihilation terms, the magnitude of the lepton pair production cross section is a sensitive test of the idea of colour.

2.4 Differential Cross Sections:

The differential forms of Equation (1) with number of colours set to three are usually written as:

$$\frac{d\sigma}{dM^2} = \frac{4\pi\alpha^2}{9M^4} F(\tau) \tag{2}$$

or

$$\frac{d^2\sigma}{dM^2 dx_F} = \frac{4\pi\alpha^2}{9M^4} F\left(\tau, x_F\right) \tag{3}$$

Here the scaling functions $F(\tau)$ and $F\left(\tau, x_F\right)$ are formed entirely from the dimensionless variables.

$$F(\tau) = \sum_i e_i^2 \tau \int dx_1 dx_2 \left[G_{q_i/A}(x_1) G_{\bar{q}_i/B}(x_2) + (q_i \leftrightarrow \bar{q}_i)\right] \delta(\tau - x_1 x_2)$$

$$F(\tau, x_F) = \frac{\tau}{\sqrt{x_F^2 + 4\tau}} \sum e_i^2 \left[G_{q_i/A}(x_1) G_{\bar{q}_i/B}(x_2) + (q_i \leftrightarrow \bar{q}_i)\right] \delta(\tau - x_1 x_2)$$

$$\times \delta\left(x_F - (x_1 - x_2)\right)$$

In the case of proton-proton collisions, one can write the function F(τ) explicitly, neglecting charmed and heavier quarks:

$$F(\tau) = \tau \int dx_1 dx_2 \; \delta(\tau - x_1 x_2) \left\{ \frac{4}{9}\left[u_A(x_1)\bar{u}_B(x_2) + \bar{u}_A(x_1)u_B(x_2)\right] + \frac{1}{9}\left[d_A(x_1)\bar{d}_B(x_2) + \bar{d}_A(x_1)d_B(x_2)\right] + \frac{1}{9}\left[s_A(x_1)\bar{s}_B(x_2) + \bar{s}_A(x_1)s_B(x_2)\right]\right\}, \quad (4)$$

where u(x), d(x) and s(x) are the probability distributions for finding the up, down and strange quark respectively with fraction x of the parent proton momentum. It is the premise of the parton model that these functions are the same as measured in deep inelastic lepton interactions. In contrast, however, to electron proton scattering, they appear in this formulae in quadratic form.

2.5 Drell-Yan Process in QCD:

Quantum Chromodynamics introduces modifications to the parton model in form of the possible emission of gluons. The first order diagrams in the strong coupling constant α_s, which contribute to the Drell-Yan process are shown in Figure 2. Of course, there are many higher order diagrams which contribute less to the cross section due to the higher powers of α_s. These are usually neglected in the phenomenological calculations. The first order diagrams correspond to the "Compton" and "Annihilation" processes respectively, where the gluon plays the role analogous to the photon in quantum electrodynamics. The subprocess variables, defined in Figure 2, are related to the overall c.m. variables through the following set of relations:

$$\hat{s} = x_1 x_2 s$$

$$\hat{t} = x_1 t + (1 - x_1)M^2$$

$$\hat{u} = x_2 u + (1 - x_2)M^2$$

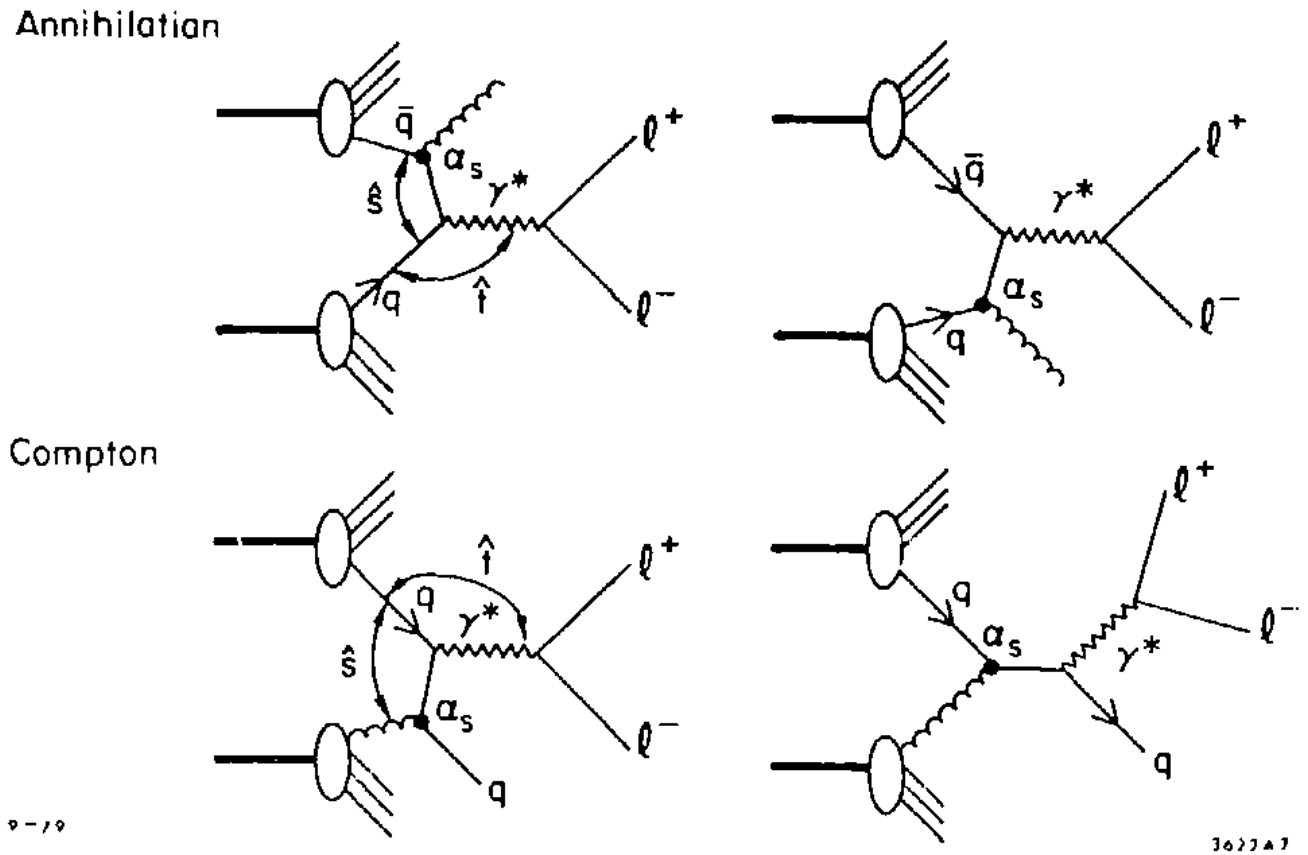

2. First order in α_s QCD diagrams contributing to the Drell-Yan process.

Here again transverse momentum of the quarks and the masses involved had been neglected. Both the "Compton" and "Annihilation" cross sections can be calculated in the field theory [7,8] and expressed in terms of the subprocess variables:

$$\frac{d^2\sigma\ (\text{Annihilation})}{dM^2 d\hat{t}} = \frac{8}{27}\,\alpha^2\,\alpha_s\,e_i^2\,\frac{2M^2\hat{s} + \hat{u}^2 + \hat{t}^2}{\hat{s}^2\,\hat{t}\,\hat{u}} \tag{5}$$

$$\frac{d^2\sigma\ (\text{Compton})}{dM^2 d\hat{t}} = \frac{1}{9}\,\alpha^2\,\alpha_s\,e_i^2\,\frac{2M^2\hat{u} + \hat{s}^2 + \hat{t}^2}{-\hat{s}^3\,\hat{u}} \tag{6}$$

Both formulae (5) and (6) are divergent for the small values of $\hat{t}$ or $\hat{u}$ and therefore are difficult to use in phenomenological applications. Politzer [9] and Sachrajda [10] have proposed a perturbative approach which includes the first order diagrams in the leading log Q^2 approximation. Here Q^2 represents the big, scale breaking dimensional quantity and is usually identified with M^2 for the Drell-Yan process.* For the $q\bar{q}$ annihilations, Politzer found that the divergent parts of the contributions due to the soft gluon emission have a factorizable form, and that they can be absorbed into the incoming particle wave function. Similar results were obtained by Sachrajda for the quark-quark, quark-gluon and gluon-gluon subprocesses. The structure functions of the parent particles become Q^2 dependent, but they are again the same as in deep inelastic lepton scattering. As the result the parton model description of the Drell-Yan process is recovered but with additional scale violating component (Figure 3).

---

* For the details of the perturbative approach to QCD, see S. J. Brodsky's lectures at this school.

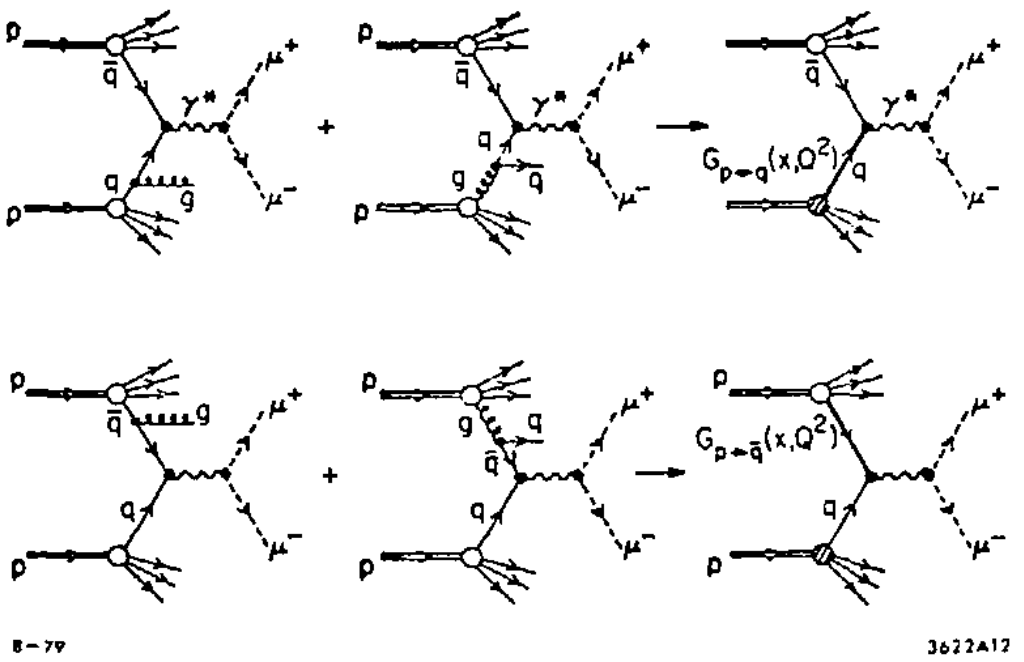

3. Illustration of the diagrams contributing to the renormalization group improved quark and antiquark distributions.

$$\frac{d\sigma}{dM^2} = \frac{4\pi\alpha^2}{9M^4} F(\tau, Q^2) \qquad (7)$$

There are several steps in this approach for which the theoretical understanding is not yet complete.

1. Diagrams of higher order in α_s contributing to the process also have similar types of divergencies in the cross sections. Although some second order terms have already been calculated, it is so far not proven that all those divergencies may be treated in the same way as in the case of the first order diagrams.

2. Non-leading terms, neglected in first approximation, may have substantial contributions to the cross section thus modifying the results.

3. The identification of the scale breaking variable Q^2 with M^2 may not be correct in the kinematical regions of phase space with two or more large dimensional variables e.g., for large mass lepton pairs produced at high transverse momentum.

4. Although in deep inelastic lepton scattering the photon is space-like $(Q^2 < 0)$ while in the Drell-Yan process it is time-like $(Q^2 > 0)$, the identification $\left|Q^2_{DIS}\right| = Q^2_{DY}$ is needed in the factorization procedure in order to deal with the same quark structure functions in both processes.

Despite those theoretical caveats, the procedure is remarkably simple and, as will be shown in the next sections, it describes most of the general features of the current experimental data.

There were recently published several papers applying the QCD phenomenology to the Drell-Yan process.[4,6-13] In general they follow the

prescription given above and differ only in the procedures for extracting scale breaking quark distributions needed as input to Eqs. (7) and (4). The accuracy of these structure functions represents a limiting factor in the phenomenology of lepton pair productions. I will return to this problem in Section 8.

3. PARTICLE TYPE DEPENDENCE

3.1 Target Dependence:

Since the density of the heavy nuclear target is much higher than that of the hydrogen, the nuclear targets are often used to study the low cross section processes. It is then an experimental problem of how to extract the cross section of a given process on nucleus from the measurements involving heavy nuclei. It has been observed in several different experiments, that the cross section has to a good approximation a power law behavior as function of the nuclear number A

$$\sigma = \sigma_0 A^{\alpha} \quad . \tag{8}$$

In coherent processes e.g., diffractive production, where one expects shadowing effects to exist, the value of $\alpha \approx 2/3$ is both observed experimentally and expected from Glauber theory. On the other hand for hard scattering processes involving partons, one does not expect any shadowing to occur. The incoming set of partons should see the target as an ensemble of point-like constituents with their number proportional to the number of nucleons, i.e., $\alpha = 1$.

The dependence of the parameter α on the mass of the $\mu^+\mu^-$ pairs produced in pN collisions is shown in Figure 4. At low mass the value of α is close to $\alpha = 2/3$. It rises with increasing mass and attains plateau consistent with $\alpha = 1$ for $M > 3$ GeV. Similar behaviour can be

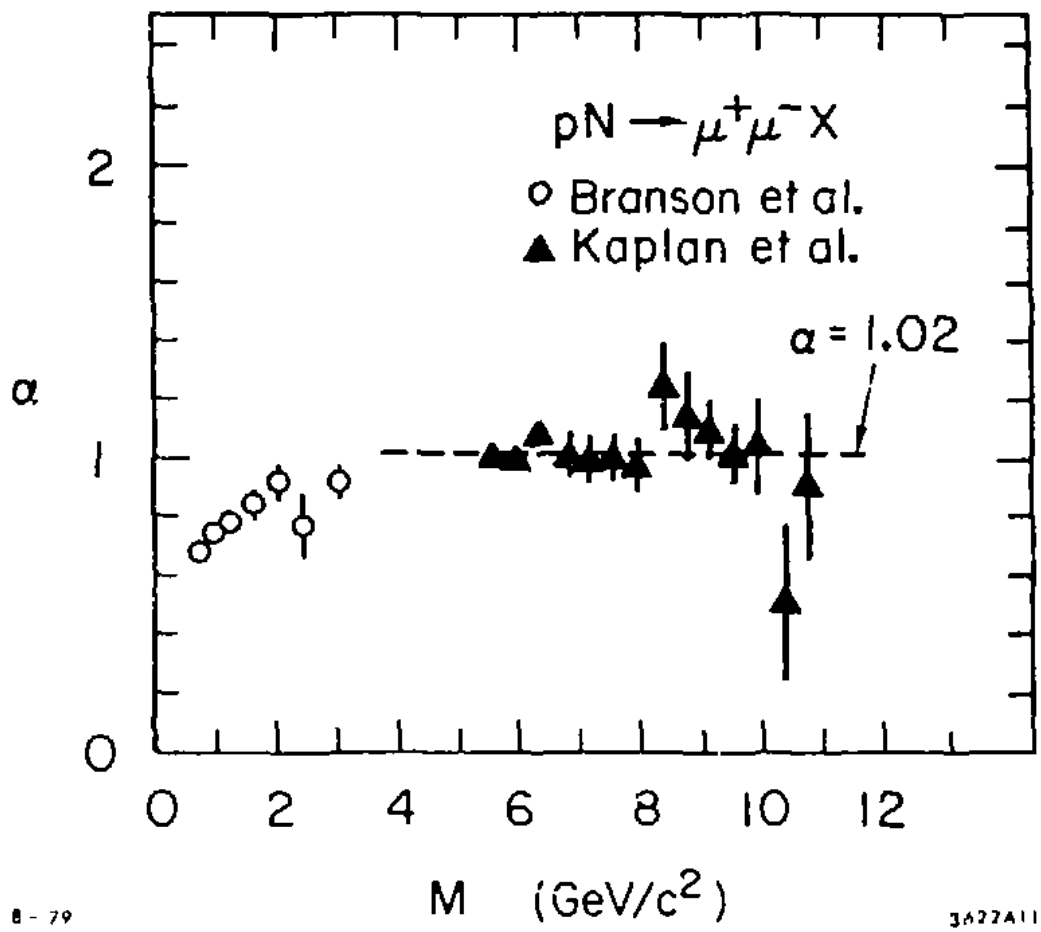

4. The atomic mass number dependence A^{α} for dimuons produced by protons.

seen in Figure 5a for the pion induced reactions. The points measured by the Chicago-Illinois-Princeton group [14] have sufficiently large errors to be consistent with the recent result of the CERN NA3 experiment, [15] giving a value of $\alpha = 1.02 \pm .02$ for $\mu^+\mu^-$ mass above 4 GeV. It is important, however, to remember that a variation of 0.10 in the α dependence corresponds to the difference of ~70% in the absolute cross section on single nucleon extracted from the measurement on a tungsten target.

As can be seen in Figures 5b and 5c, the parameter α has no obvious p_T or x_F dependence for the high $\mu^+\mu^-$ mass indicating that the normalization of the cross section is independent of the kinematics.

There is a natural interpretation of the observed effects: At low lepton pair mass the Drell-Yan process represents only a small fraction of the total cross section. Other coherent mechanisms and absorptive effects contribute substantially to the cross section, thus masking the characteristic features of the hard process. At higher mass, however, those other processes may be assumed to be negligible and the Drell-Yan mechanism dominates. The study of the target mass dependence defines, therefore, the region of applicability of the Drell-Yan description of massive lepton pair production. Only the region where $\alpha = 1$, i.e., for $M > 4$ GeV, can be used for tests of the parton model and QCD calculations of the Drell-Yan process.

3.2 Beam Dependence:

One of the first qualitative successes of the parton model description of the Drell-Yan process was the observation of the effects expected for various incoming beams. For the isoscalar nuclear targets one usually neglects the contribution of the sea component to the annihilation process. With such assumption the relative yield of lepton pairs

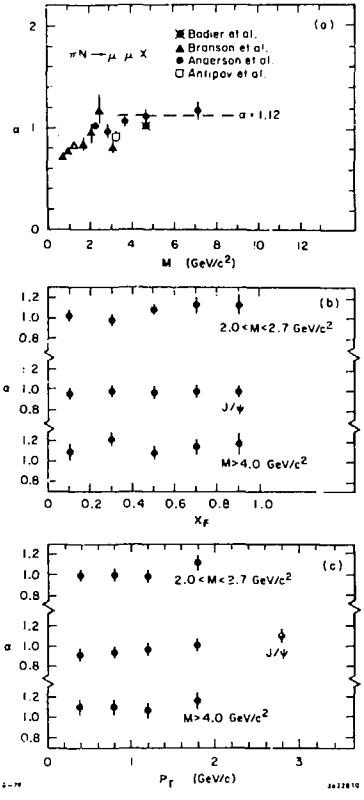

5. The dependence of the parameter α on: a) mass, b) Feynman x, c) transverse momentum of muon pair produced by pion beam.

depends only on the quark content of the beam. Figure 6 shows the ratio R_1 of muon pair production in π^+N and π^-N interactions as a function of mass of the $\mu^+\mu^-$ pair.[14,15] In the region where the sea of the pion may be neglected i.e., at large values of x (which correspond to high mass), the value of R_1 should approach the ratio of the charges squared of the annihilating antiquarks.

$$R_1 = \frac{\sigma(\pi^+N \to \mu^+\mu^-X)}{\sigma(\pi^-N \to \mu^+\mu^-X)} \xrightarrow{\text{at high } x} \frac{e_{\bar{d}}^2}{e_{\bar{u}}^2} = \frac{1}{4} \quad .$$

The data in Figure 6 show a clear trend confirming such expectations. The value of R_1, expected from the contribution of the sea to be equal to 1 at low x, decreases with increasing mass and is compatible with 1/4 at large x. The energy dependence of the decrease reflects variation of the range of x contributing to fixed values of $\mu^+\mu^-$.

More dramatic effects are expected for the ratio of pion and proton interactions producing lepton pairs. In pN collisions the annihilating sea antiquark is confined to small values of x. Therefore the cross section is expected to decrease sharply with increasing mass. On the other hand, the incoming pion has a valence antiquark thus providing a larger x (or mass) range for the Drell-Yan process.

The ratio of the muon pair production by the pion and proton beams is shown in Figure 7. It exceeds the value of 100 for masses above 10 GeV reflecting the difference of the antiquark x distributions.

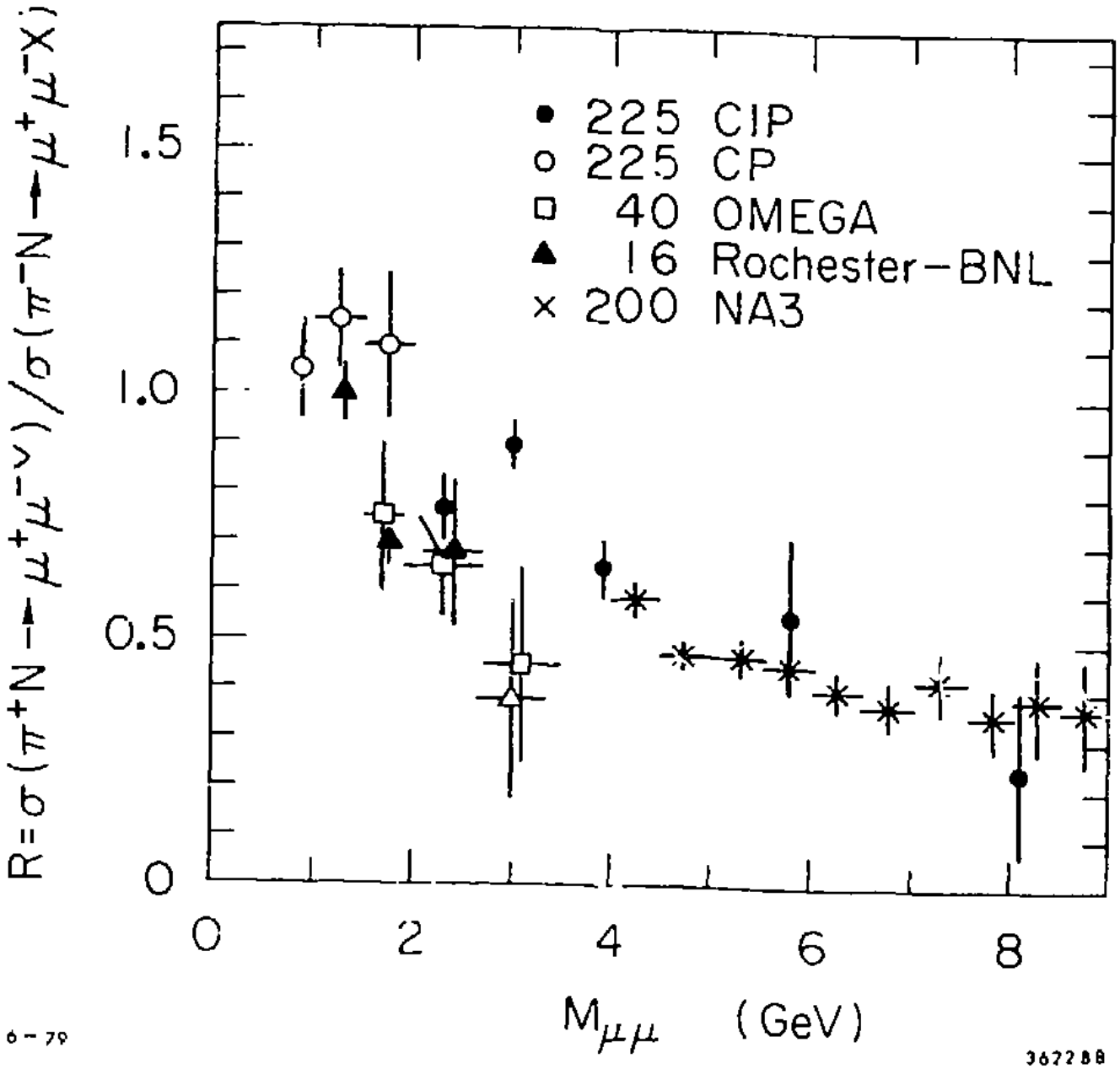

6. Ratio of the dimuon production cross section in π^+N and π^-N interactions versus $M_{\mu^+\mu^-}$.

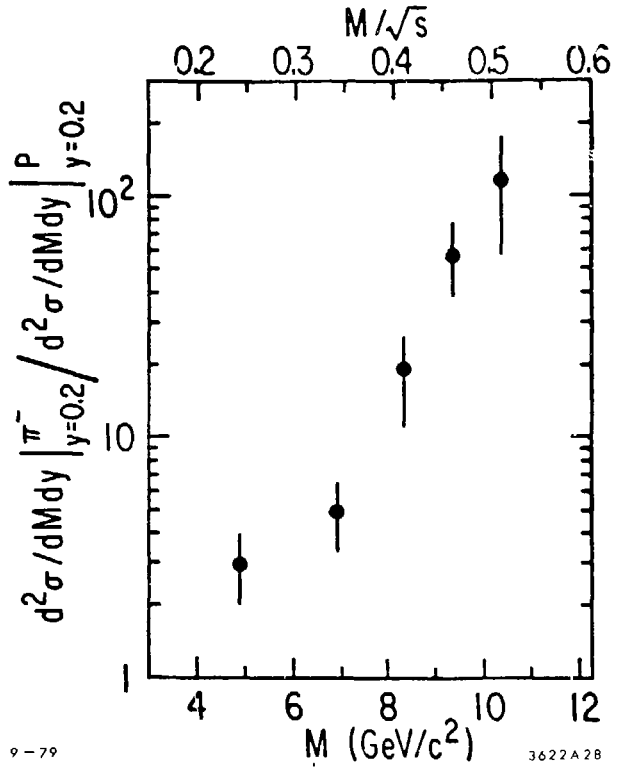

7. The ratio of π^- induced to proton induced $\mu^+\mu^-$ pair cross sections at $y_{cm} = 0.2$ as function of mass.

4. MASS SPECTRA

4.1 pN Interactions:

The $\mu^+\mu^-$ mass distribution shown in Figure 8 represents one of the most impressive measurements of the high energy experiments of the last few years. The Columbia-Fermilab-Stony Brook results span almost ten orders of magnitude of the cross section and extend to mass of about 20 GeV. The mass resolution allows for clear separation of vector mesons from the Drell-Yan continuum. Several groups have measured this spectrum at various energies. The compilation of results presented in form of the scaling function $F(\tau)$ is shown in Figure 9. The Fermilab data are well parameterized [3] by the formula

$$s \left.\frac{d^2\sigma}{d\sqrt{\tau}\, dy}\right|_{y=0} = 44.4\, e^{-26.6\sqrt{\tau}} \quad \mu b \quad , \tag{9}$$

while the CHFMNP group [18] at the ISR obtained the best fit to the data with

$$M^3 \frac{d\sigma}{dM\, dx} = 5.23 \frac{(1-\sqrt{\tau})^{10}}{\sqrt{\tau}} \times 10^{-33} \ (cm^2 GeV^2) \quad . \tag{10}$$

It is evident from Figure 9 that the tests of scaling over the large energy range are very difficult. Low energy data are limited to the mass range below 3 GeV, where other than Drell-Yan processes contribute. On the other hand the ISR measurements are concentrated at small values of τ. The best test of scaling existing so far is shown in Figure 10, where the 200, 300 and 400 GeV/c pN results of the CFS group [17] are presented. The agreement with scaling, to within the 20% errors of the ratios, is not in contradiction with the expectations of QCD, that scale breaking should occur. The measurements of

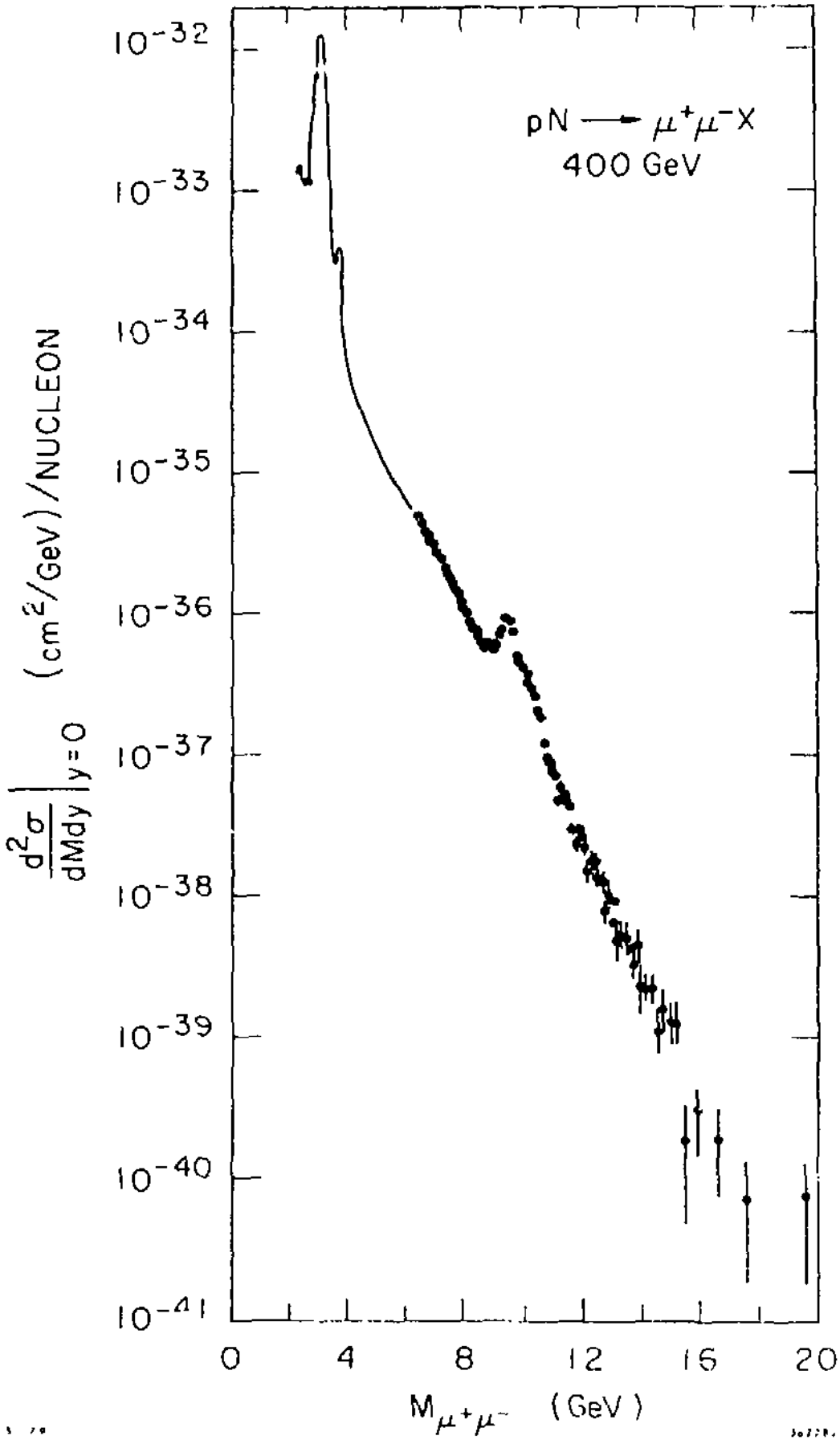

8. Dimuon spectrum measured by the CFS Collaboration. Solid line describes the 1976 data; data points are from Reference 17.

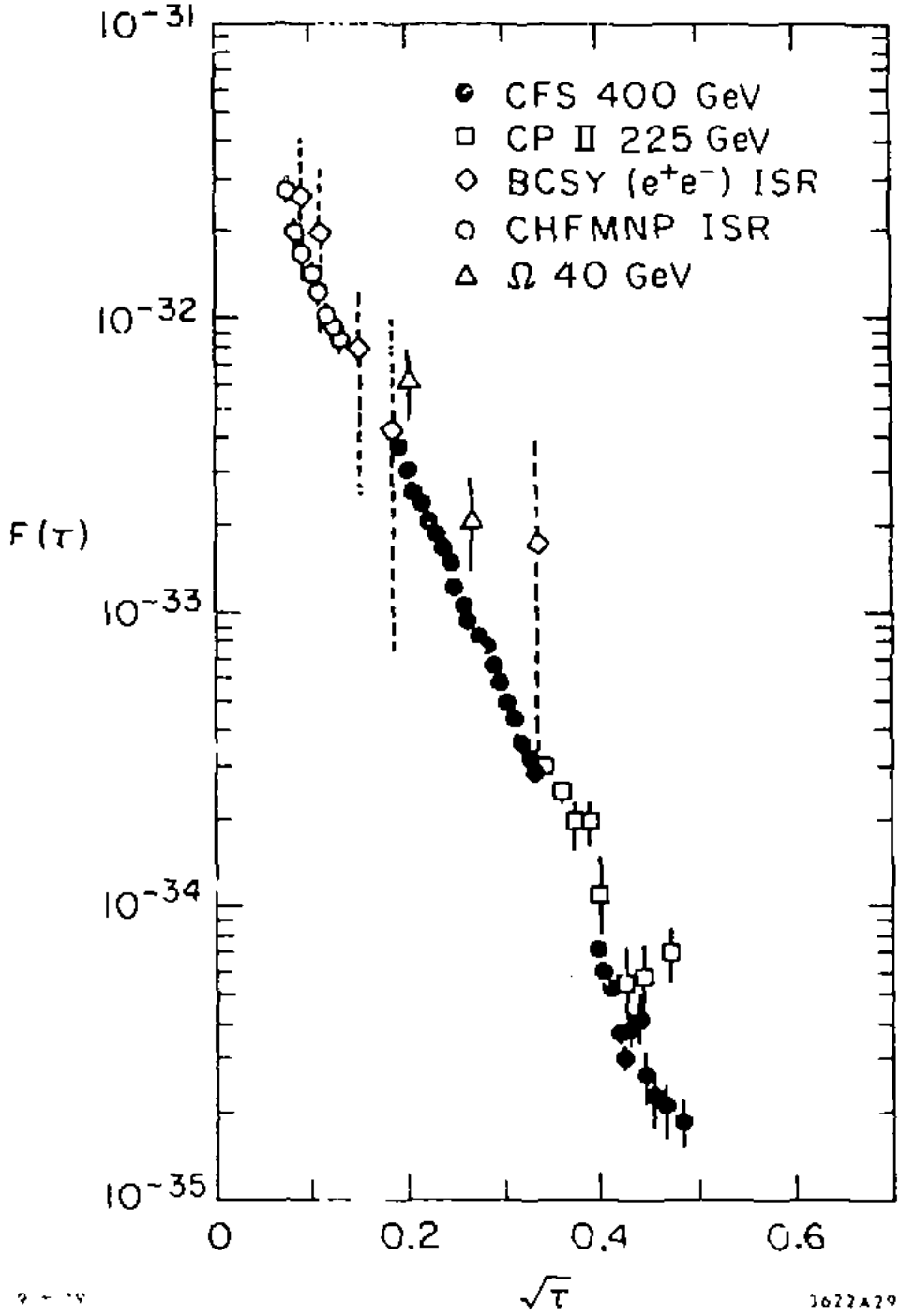

9. The experimental function $F(\tau)$ versus $\sqrt{\tau}$ for the dileptons produced by protons.

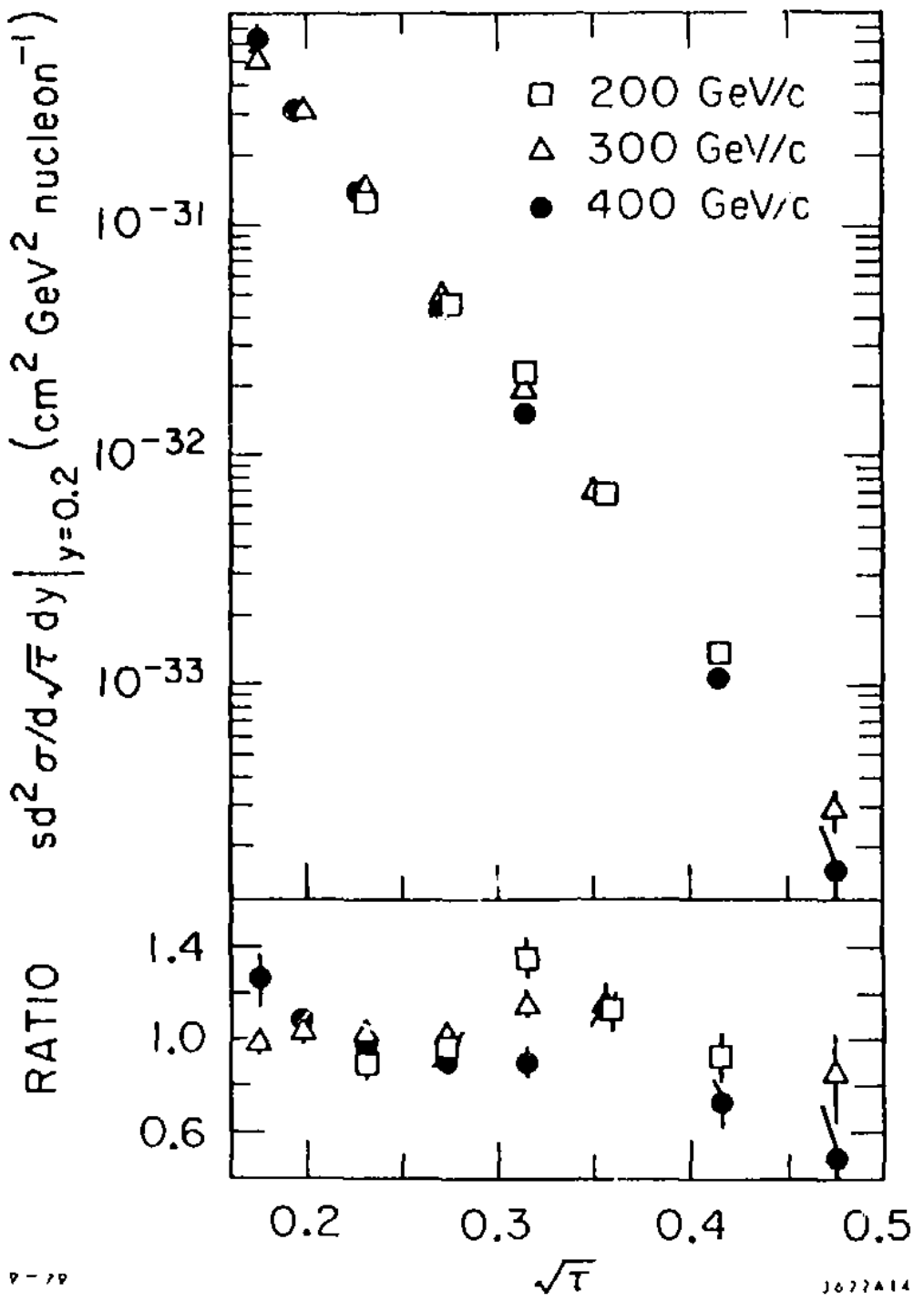

10. Scaling function and the corresponding ratios at 200, 300 and 400 GeV/c.

the CFS collaboration were done at $y \approx 0$ where, for the pp interactions, the x values of the annihilating quarks are approximately equal to $\sqrt{\tau}$. Since the pattern of scale breaking of mass distributions follows that of the structure functions, one expects no scaling violations for $\sqrt{\tau} = 0.2$ and the decrease of $F(\tau)$ with increasing energy for $\sqrt{\tau} > 0.2$. The data in Figure 10 agree with such behavior.

4.2 πN Interactions:

Until recently the spectra of lepton pairs produced in πp collisions were available mostly at low masses. The Rochester-BNL collaboration[16] have estimated the relative contribution of the Drell-Yan mechanism to the observed $\mu^+\mu^-$ mass distributions produced in 16 and 22 GeV/c π^-p interactions. As can be seen in Figure 11, the competing processes contribute over 50% of the measured spectrum below 3 GeV/c^2 making any tests of scaling without detailed knowledge of those mechanisms impossible.

This summer, however, first results became available from the new experiments both at Fermilab[14] and CERN.[15] As can be seen in Figure 12 the cross section measured is much larger than that for the proton induced reactions. This effect was already seen in Figure 7. It reflects the difference of the pion and proton structure functions. The pion induced data are summarized in Figure 13. The shape of the distribution measured by various experiments is similar. The discrepancy in the relative normalizations can be attributed mainly to the different target mass dependence used by the experimenters in order to extract the cross section on single nucleons.

The data at 200 and 280 GeV/c were, however, measured in the same experiment, thus eliminating most of the relative normalization

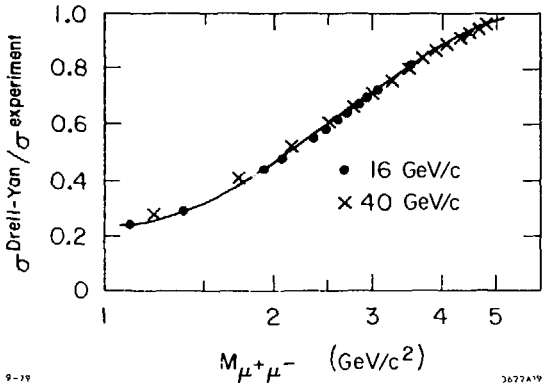

11. The fraction of dimuons produced by the Drell-Yan mechanism as a function of $M_{\mu^+\mu^-}$.

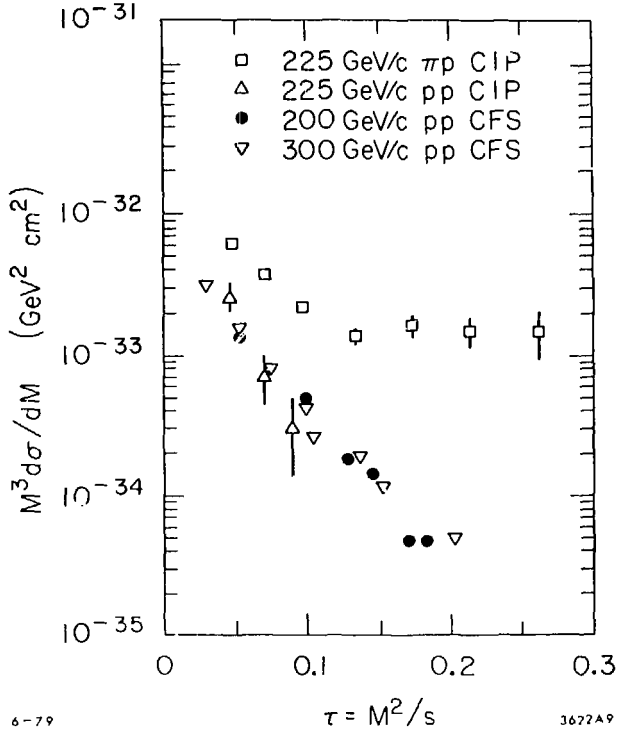

12. Comparison of the scaling functions for the pion and proton induced dimuons.

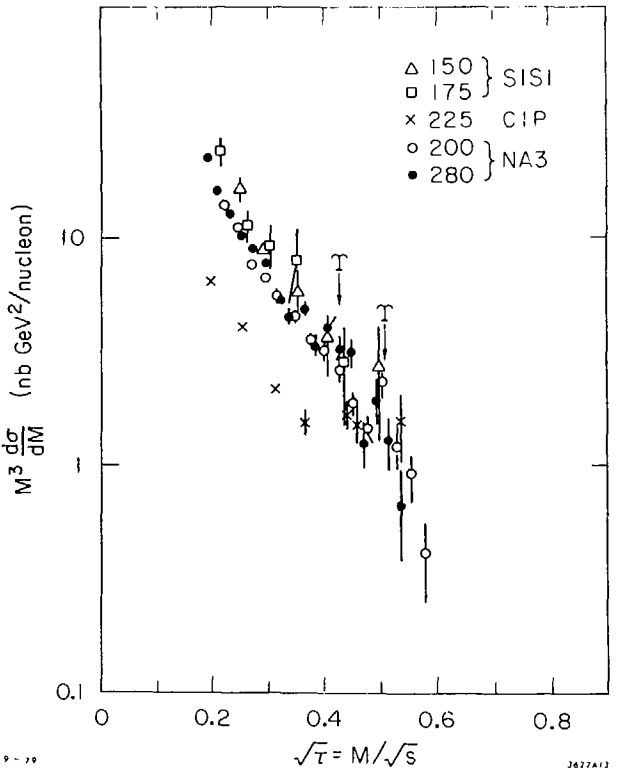

13. Compilation of the $F(\tau)$ versus $\sqrt{\tau}$ for the pion produced dimuons.

problems. Within their 15% errors they show good scaling over large τ range except in the upsilon region.

5. MOMENTUM SPECTRA OF LEPTON PAIRS

5.1 Longitudinal Momentum Distributions.

The difference of the shapes of the antiquark structure functions of pion and proton are also reflected in the longitudinal momentum distributions of the lepton pairs. In Figure 14 are presented the x_F distributions measured by the Chicago-Illinois-Princeton collaboration.[14] The data are parametrized as

$$E \frac{d\sigma}{dx_F} = A(1 - x_F)^{\beta} \quad , \tag{11}$$

with the parameter β fitted in the range $0.2 \leq x_F \leq 1.0$.

There are two obvious observations to be made:

i) the value of β is much smaller for the pion data than for the proton induced results, and

ii) there is a strong decrease of the value of β with increasing mass of the lepton pair.

Similar behavior was also seen in other experiments.[15,16] Both of those observations reflect the fact that the x distribution of the annihilating valence quarks in the pion is harder than that of the quarks in the proton.

The small asymmetry around $x_F = 0$ in pN reactions[17,18] may be explained by the asymmetry of the quark content of the beam and target systems. The isoscalar targets have equal number of protons and neutrons i.e., equal number of up and down quarks, while the incoming proton has two up and only one down valence quark. The weights given by the squares of the corresponding quark charges in the formula (4) introduce the asymmetry in the longitudinal momentum distribution.

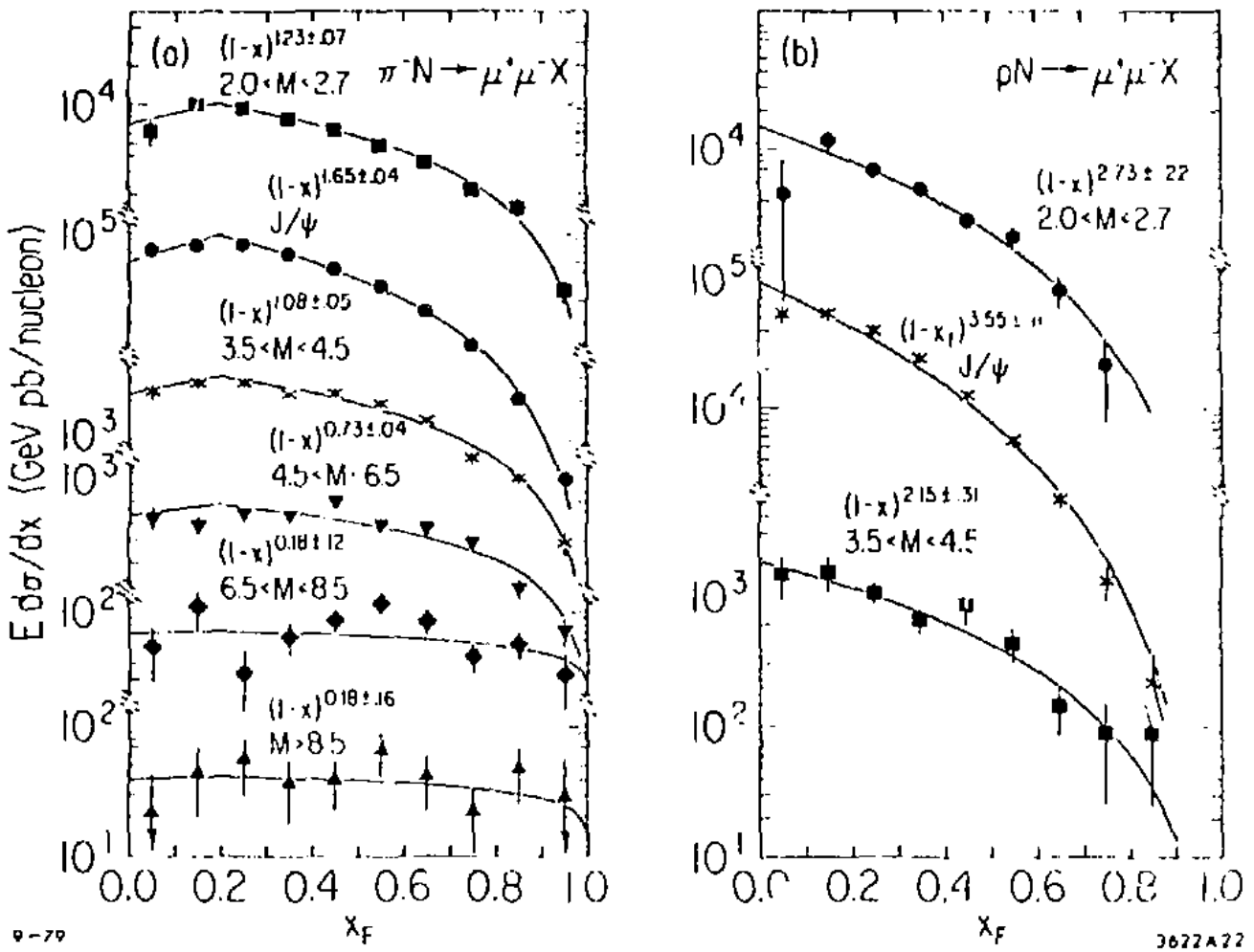

I4. Invariant x_F distribution as the function of the dimuon mass produced by: a) pions and b) protons.

5.2 Transverse Momentum Distributions:

In the simple Drell-Yan mechanism, the transverse momentum of the virtual photon is related to the transverse momentum of the annihilating quarks. In the parton model such transverse momentum is related through the uncertainty principle to the size of the parent hadron and is expected to be of the order of about 300 MeV/c. It was, therefore, a surprise when the observed transverse momentum of the lepton pairs was found to be large at large masses and to increase with s.

The example of the p_T^2 distribution of the dimuon is shown[19] in Figure 15. The data deviate strongly from the exponential behavior both in terms of p_T and of p_T^2, and are well parametrized[3,19] by the formula:

$$E\,\frac{d^3\sigma}{dp^3} = c\left[1+\left(\frac{p_T}{p_o}\right)^2\right]^{-6} \qquad (12)$$

The parameter p_o is very little dependent on mass and x_F, but it does depend on energy.

The changes of the shape of the p_T distributions are probably best visible in plots of the average transverse momentum, $\langle p_T\rangle$, versus the mass of the lepton pair. The compilation of the available data for the proton beams is shown in Figure 16. The data points raise from about 600 MeV/c at low $\mu^+\mu^-$ mass to values exceeding 1.0 GeV/c at higher masses. For M > 4 GeV the average transverse momentum seems to saturate. There is, however, quite strong energy dependence of the developed plateau. This is illustrated in Figure 17, where for the mass range of $6 < M(\mu^+\mu^-) < 8$ GeV the average transverse momentum at 200, 300 and 400 GeV/c [17] is compared with preliminary ISR results of the CERN-Harvard-Frascati-MIT-Naples-Pisa Collaboration.[10] The linear $\langle p_T\rangle$ dependence on

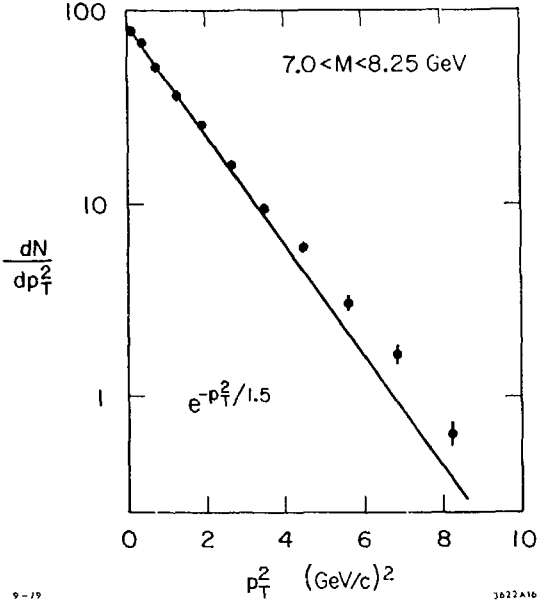

15. p_T^2 distribution of the muon pairs.

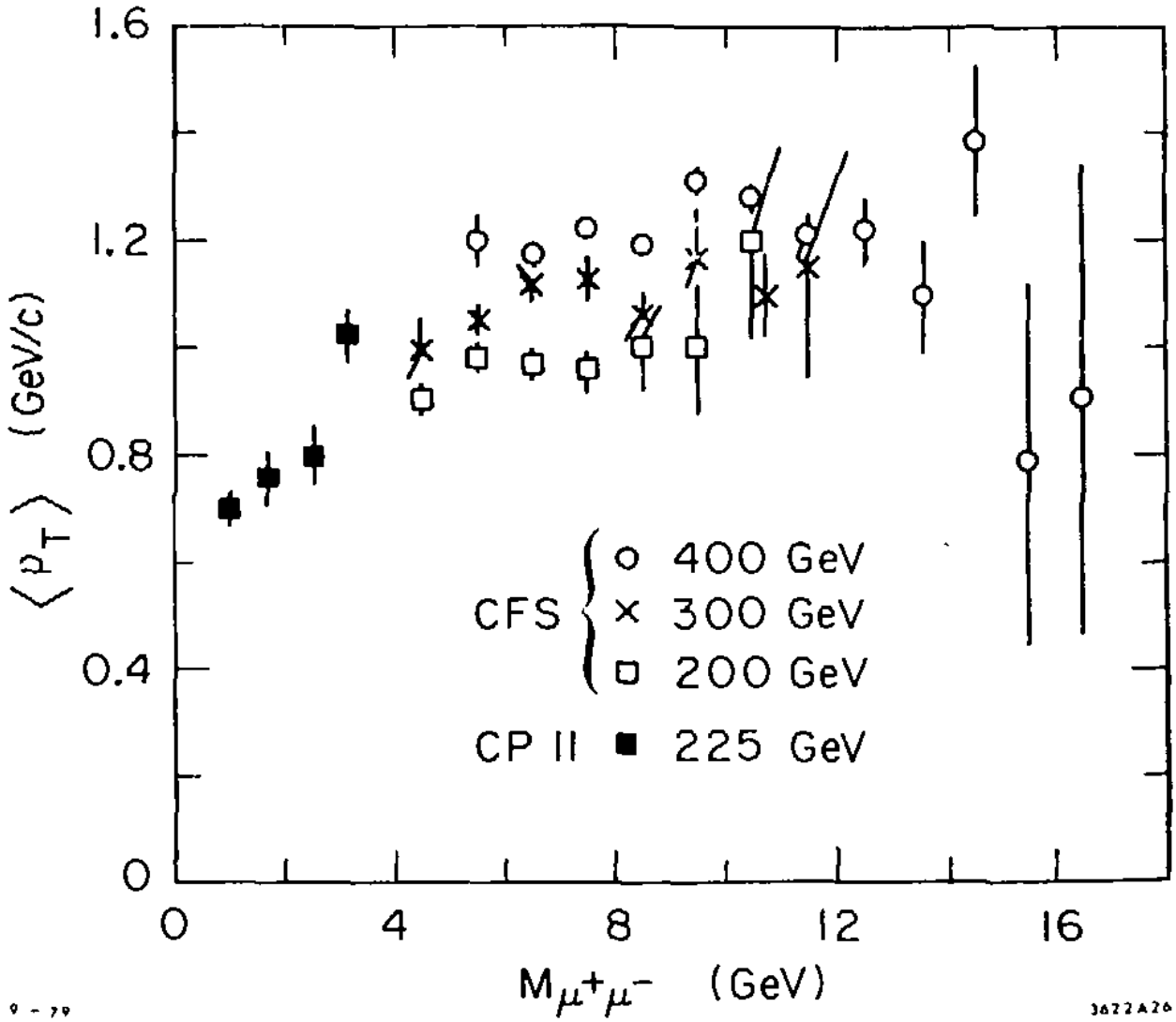

16. Average transverse momentum as function of $M_{\mu^+\mu^-}$ for the pN interactions.

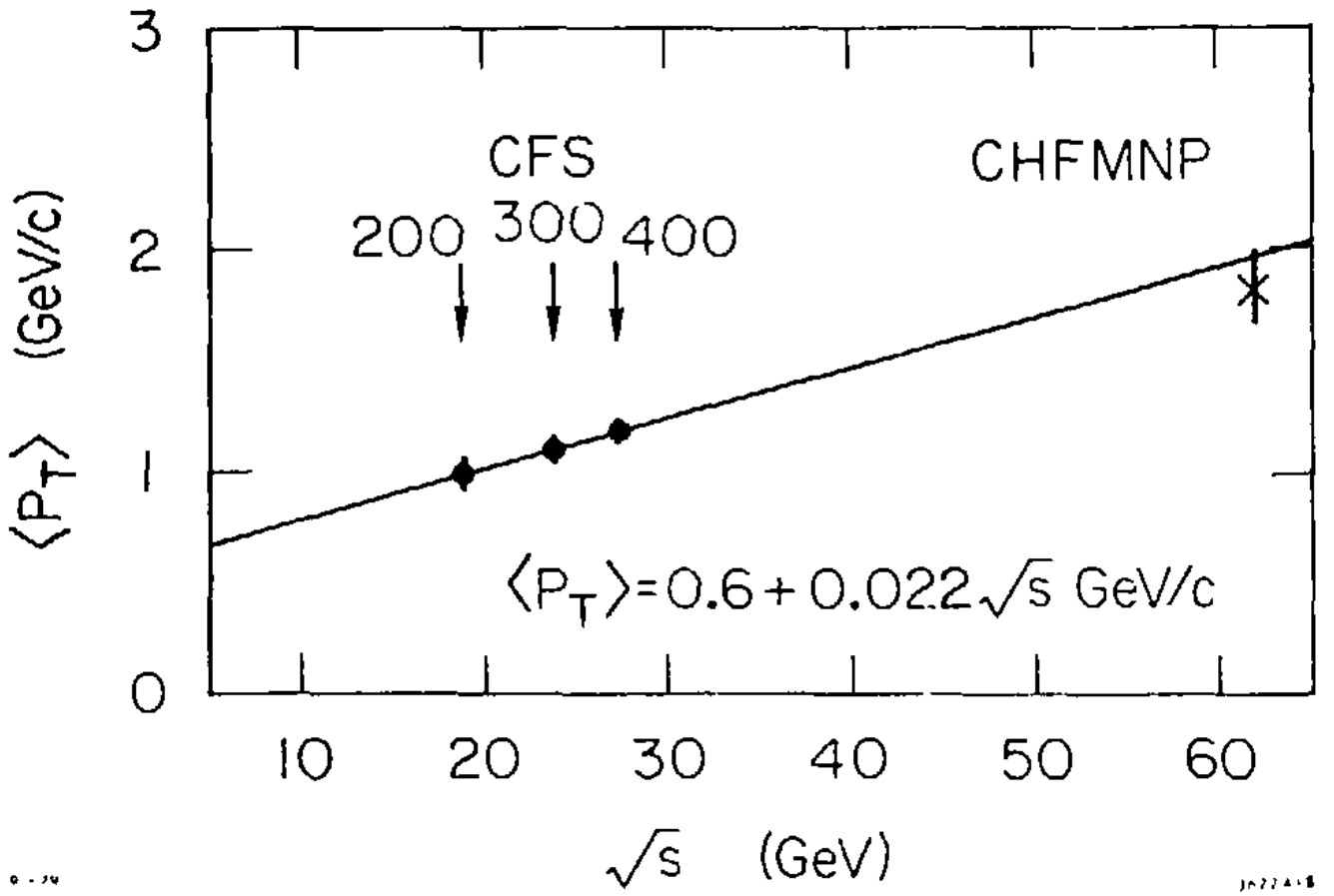

17. Energy dependence of the average transverse momentum.

The c.m. energy s:

$$\langle p_T \rangle = 0.6 + 0.022 \sqrt{s} \qquad (13)$$

is compatible[4,20] with the expectations of the QCD. It is worth noting that if this behaviour continues at higher energies, the average transverse momentum of the lepton pairs at e.g., $\sqrt{s}$ = 800 GeV would be of the order of 18 GeV/c, thus introducing serious background to the search of the intermediate vector boson.

The average transverse momentum of the muon pairs produced by the pion beams is compared in Figure 18 with that for the proton induced reactions. It shows basically the same characteristic behaviour. The level of the plateau at higher masses is, however, about 200 MeV/c higher than in the pN collisions again reflecting harder x spectrum of pion consitutents.

6. QCD PHENOMENOLOGY OF LEPTON PAIR PRODUCTION

Until recently most of the features of the lepton pair data, such as beam dependence, scaling, longitudinal momentum distribution, etc., were well described by the Drell-Yan parton model. The need for the departure from such a simple picture is, however, indicated by the large transverse momentum of the lepton pairs. The QCD procedure described in Section 2.5 was used by several authors [4,7,12,20,21] to calculate the first order diagrams predictions for the Drell-Yan process. The calculations required as input the individual quark structure functions, which had to be extracted from the deep inelastic lepton scattering data. Although the nucleon structure function νW_2 is quite well measured, its decomposition into the quark distributions is, so far, rather poorly known. Nevertheless, the agreement of such calculations with the measured mass

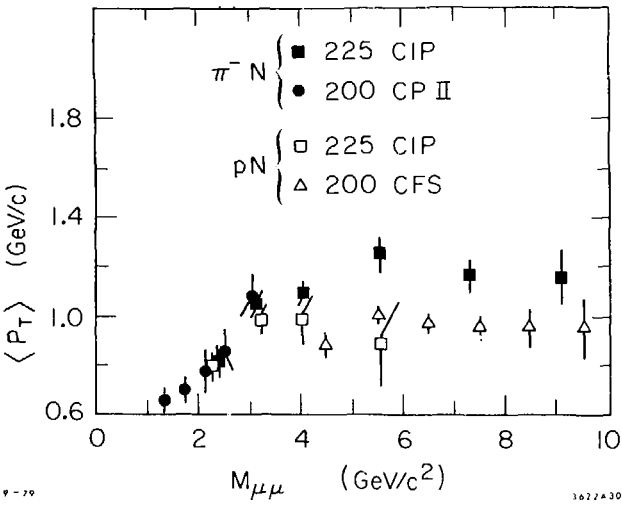

18. Comparison of the mass dependence of $\langle p_T \rangle$ for dimuons produced by π^- and proton beams.

spectra and the longitudinal distributions seems to be quite satisfactory,[22] thus reproducing the success of the parton model. The transverse momentum distributions require, however, a more complicated approach.

In the perturbative QCD the virtual photon acquires its transverse momentum through the emission of hard gluons. The first order in α_s diagrams can be calculated according to formulae (5) and (6). Their contribution to the total p_T spectrum is shown in Figure 19. In the region of small transverse momenta, where both "Annihilation" and "Compton" contributions diverge, one can argue that the non-perturbative, confinement phenomena dominate. Nevertheless, even above $p_T = 1$ GeV/c, the contribution of the first order diagrams is about factor of two smaller and has the curvature opposite to that of the data. This does not mean, however, that the QCD is necessarily failing to describe the Drell-Yan process. There are in the literature several ways of explaining this problem.

1. "Primordial" transverse momentum. It is proposed[8,12,24] that the intrinsic, non-perturbative, transverse momentum due to the quark confinement in the original hadron is, for some unspecified reason, large. The observed p_T of the lepton pair is then described by the incoherent sum of the primordial component and the contribution of the perturbative QCD. The confinement transverse momentum is in such approach, usually parametrized as Gaussian, with the average k_T varying from 0.6 to 1.5 GeV/c, depending on the analysis. The results fit the data (see Figure 20), but there is no good explanation of why the primordial transverse momentum is so large.

2. "Higher twist" effects. The Constituent Interchange Model approach[25,26] is used to account for the neglected higher order in

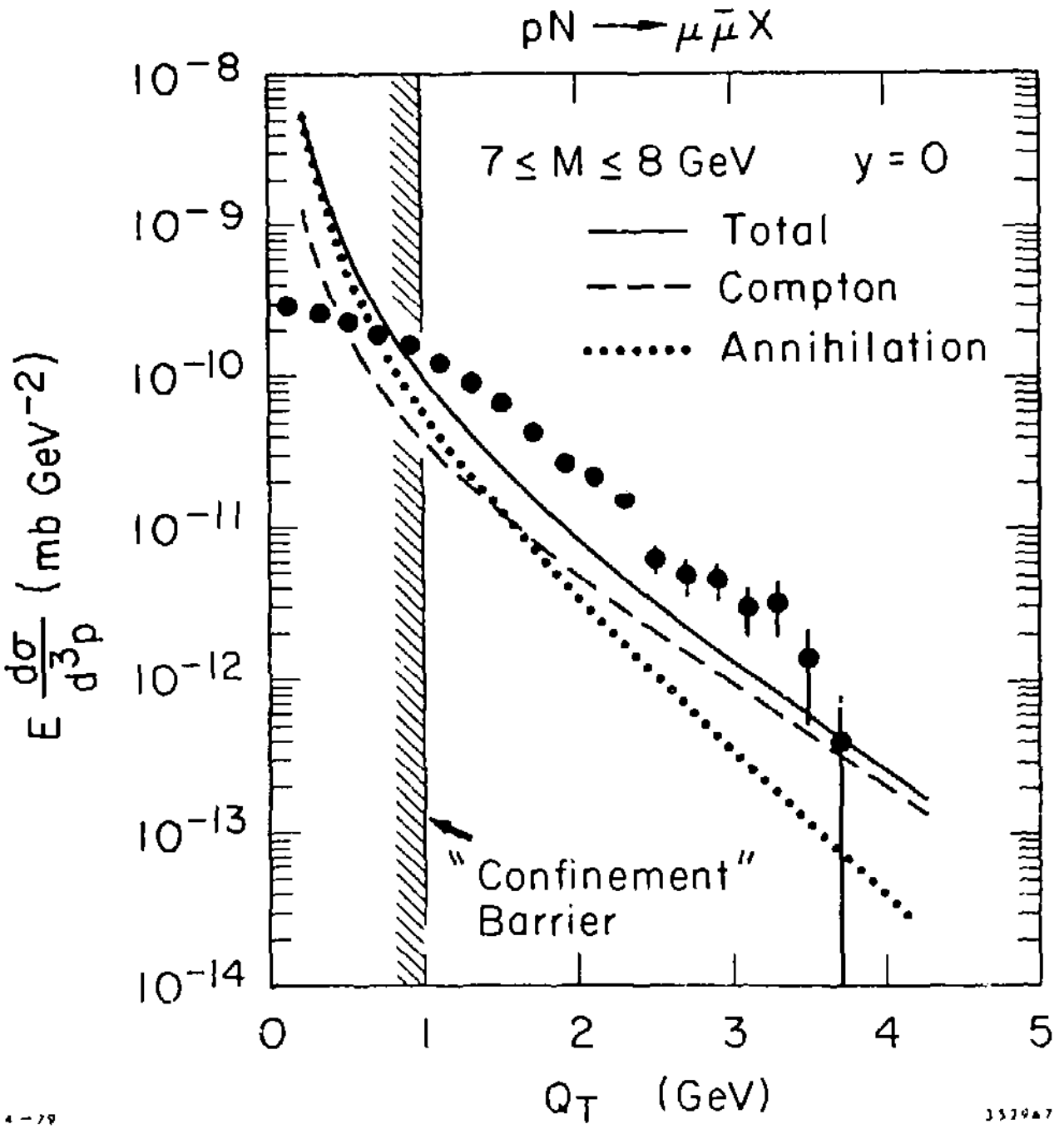

19. Comparison of the QCD calculations of dimuon transverse momentum by Berger (Reference 4) with CFS data.

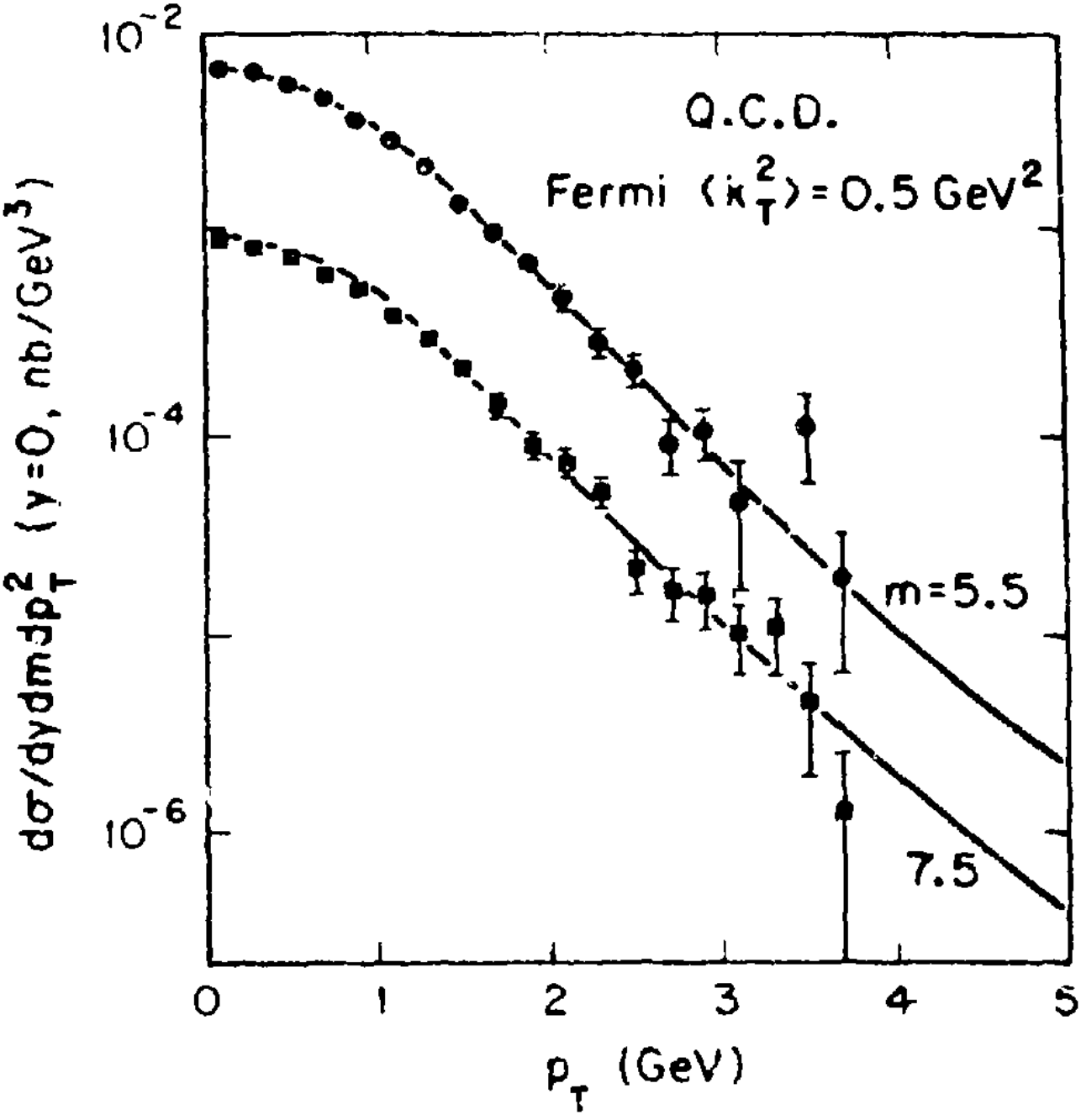

9 − 79 3622A31

20. Halzen and Scott fit (Reference 24) to the dimuon transverse momentum distribution.

α_s terms. This approach stresses the quasi-bound structure of the incoming hadrons by emphasizing the meson-quark or diquark-quark subprocess contributing to the reaction. The model introduces effective coupling of mesons to quarks and unknown distributions of mesons inside the hadrons,[27] but it successfully fits the data on the lepton pair production (Figure 21).

3. An interesting, but also difficult, approach had been chosen by Dokshitser, Dyakonov and Troyan[28] who have calculated the QCD terms to all orders in α_s in the leading log Q^2 approximation. They have obtained a solution in the kinematical region of $p_T^2 >> M^2$, though the identification of the scale breaking variable Q^2 in the region of two large dimensional variables (p_T and M) is unclear. So far there is no experimental data available for $p_T >> M$.

Independently of the various schemes described above, it is clear from Figure 19 that the measurements of the lepton pair production at very large p_T will provide a sensitive test of QCD. In this region the higher order corrections are expected to be negligible and numerical comparison of the first order calculations with the data will be possible.

It is also interesting to note that in the pN reactions the "Compton" diagrams dominate at large transverse momentum; i.e., p_T of the lepton pair is balanced by the recoiling quark (see Figure 2). On the other hand, for the πN interactions the contribution of the "Annihilation" diagrams is much larger than than of the "Compton" graphs, requiring recoiling gluon to balance p_T. Therefore the measurements of hadrons accompanying high mass lepton pairs produced at large p_T may provide an opportunity to study quark and gluon jets.

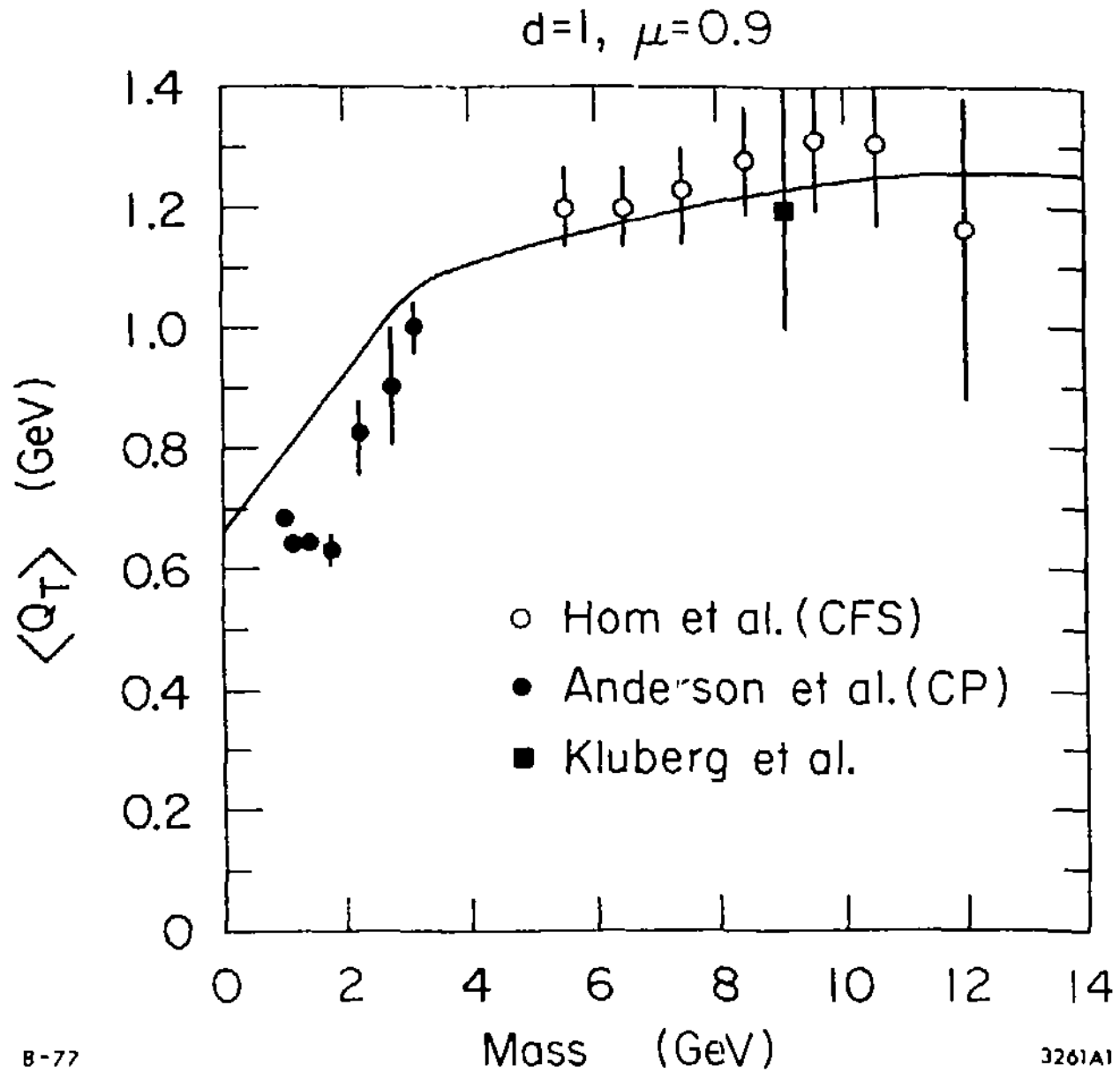

21. CIM description of the $\langle p_T \rangle$ dependence (Reference 25).

7. ANGULAR DISTRIBUTIONS

The general form of the angular distribution for the decay of the virtual photon into lepton pair may be written[29] as:

$$W(\Theta^*,\phi) = \frac{3}{8\pi}\left[\rho_{11}\left(1+\cos^2\Theta^*\right) + \left(1-2\rho_{11}\right)\sin^2\Theta^* + \rho_{1-1}\sin^2\Theta^*\cos 2\phi + 2\,\mathrm{Re}\,\rho_{10}\sin 2\Theta^*\cos\phi\right], \quad (14)$$

where the density matrix elements ρ_{ij} depend on the choice of the reference frame and all the variables describing the virtual photon, i.e., M^2, x_F, p_T, s. Integration over either polar or azimuthal angle gives:

$$W_1(\Theta^*) \sim 1 + \alpha\cos^2\Theta^* \quad , \quad (15)$$

$$W_2(\phi) \sim 1 + \beta\cos 2\phi \quad , \quad (16)$$

where both α and β may vary between -1 and $+1$.

There are several ways of defining the axes in the rest frame of the lepton pair. The usual choice is the Gottfried-Jackson frame, where Θ^* is the angle between the beam and one of the leptons. This reference frame is well suited for testing of the Drell-Yan process when the direction of the quarks coincides with the direction of the beam. The primordial transverse momentum of the quarks may, however, introduce additional smearing effects to the angular distributions, as the direction of the beam and of the annihilating quarks will no longer overlap. To deal with this problem Collins and Soper[30] have proposed a reference frame in which the z axis bisects the angle between the beam and reverse target momentum directions in the lepton rest system. Such axis should minimize the smearing effects if the primordial transverse

momentum distributions of the beam and target quarks are similar. Experimentally, the Collins-Soper frame is found to be very close to the Gottfried-Jackson reference system. In the $\pi^- N$ interactions at 225 GeV/c the average angular difference between the two z axes was estimated [31] to be about 14^0.

The data of the Chicago-Illinois-Princeton Collaboration [31] are shown in Figure 22. The angular distribution, integrated over the polar angle ϕ, is considerably different in the region of the Drell-Yan continuum than for the J/Ψ resonance. The data are plotted as function of the x_1 of the annihilating valence quark of the pion. In each of the intervals the form (15) is a good representation of the data, but the parameter α shows strong x_1 and p_T dependence (see Figure 23). The deviations of α from the value of $\alpha = 1$ indicate existence of the longitudinal polarization of the virtual photon.

Two possible origins of the deviations from purely transverse polarization of the virtual photon has been discussed recently in the QCD framework.

1. First order in α_s "Compton" subprocesses, in which quark interacts with spin 1 gluon, were shown [21,32] to lead to $\sin^2\Theta^*$ behavior. In this case a non-trivial azimuthal dependence is also expected, and the parameter β in formula (16) is related [21] to α through

$$\beta = \frac{1-\alpha}{2(3+\alpha)}$$

The solid curve in Figure 23a representing the prediction of Ref. 21 is in good agreement with the data.

2. Another approach was taken by Berger and Brodsky [33] who introduced the correlations between the valence quarks in the pion

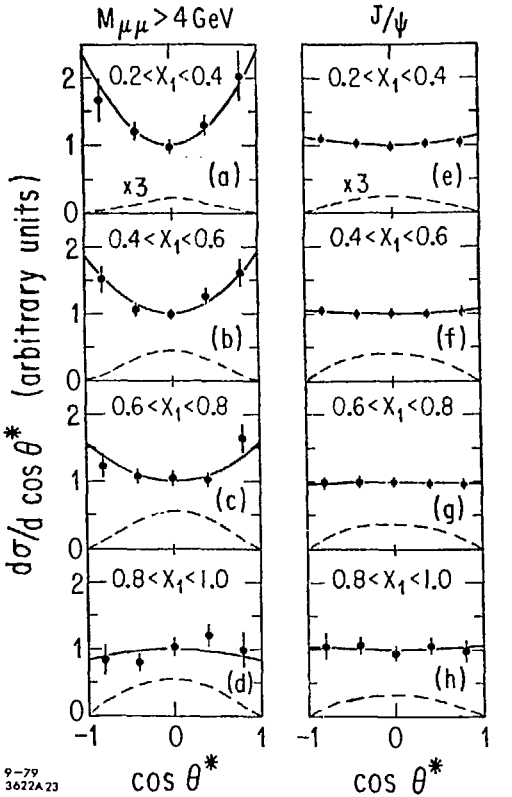

22. Angular distribution of the dimuons for various intervals of the fractional momentum x of the pion antiquark.

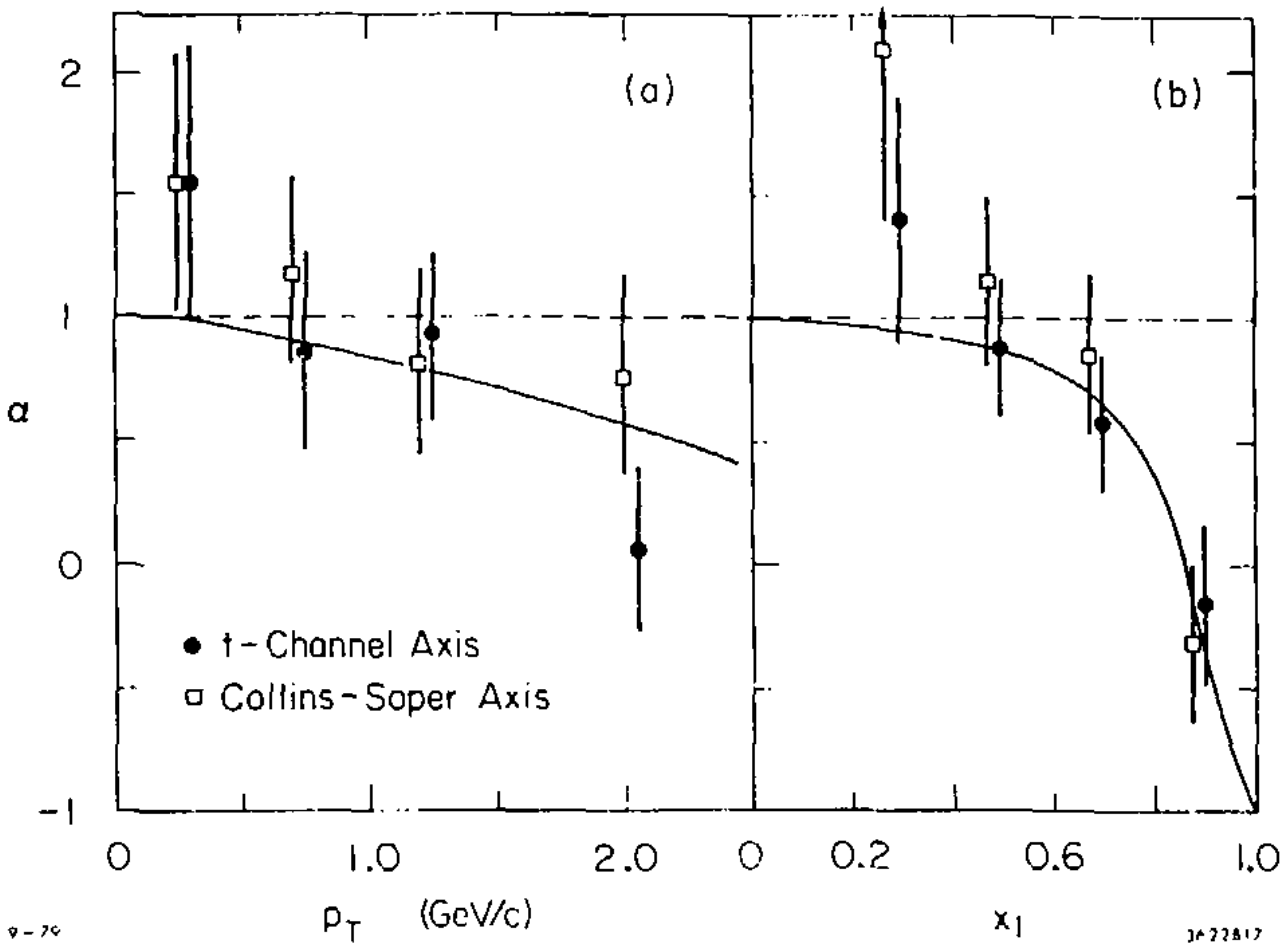

23. Dependence of the parameter α on:

a) transverse momentum of dimuons,

b) fractional momentum x of the pion antiquark.

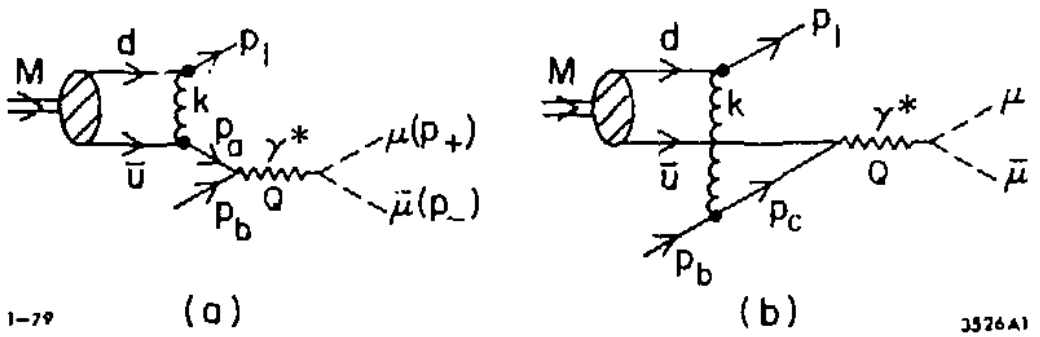

24. Diagrams for $Mq \to q\gamma^*$, $\gamma^* \to \mu^+\mu^-$ used in calculations of Berger and Brodsky (Reference 33).

calculating the "higher twist" terms of Figure 24. The resulting decay angular distribution is predicted to vary strongly with Q^2 and x_F of the virtual photon:

$$d\sigma \sim (1-x)^2 (1+\cos^2\Theta^*) + \frac{4}{9} \frac{\langle k_T^2 \rangle}{Q^2} \sin^2\Theta^* + \frac{2}{3}\sqrt{\frac{k_T^2}{Q^2}} (1-x) \sin 2\Theta^* \cos\phi \qquad (17)$$

For fixed values of Q^2 the parameter α of Eq. (15) is expected to approach -1 as x approaches 1. The prediction is compared with the data in Figure 23b. It is important to note that the "higher twist" approach predicts $\beta \simeq 0$. Therefore, the study of the experimental ϕ distributions and their correlations with the polar angle Θ^* behavior as function of M, x and p_T, may provide the opportunity to estimate the relative size of both first order and higher order contributions.

8. STRUCTURE FUNCTIONS AND QUARK DISTRIBUTIONS

8.1 Parton Model:

In the parton model the scaling function $F(\tau)$ depends on the x distributions of the individual quarks. In the case of e.g., pN collisions and neglecting heavy quark contributions, there are six unknown functions. These are $u(x)$, $d(x)$, $s(x)$, $\bar{u}(x)$, $\bar{d}(x)$ and $\bar{s}(x)$. The antiquarks come only from the sea while the u and d quarks have both sea and valence components. Taking into account the isospin invariance, the deep inelastic lepton scattering measurements provide[34] six equations:

$$\nu W_2^{ep}(x) = \frac{4}{9} x\left[u(x)+\bar{u}(x)\right] + \frac{1}{9} x\left[d(x)+\bar{d}(x)\right] + \frac{1}{9} x\left[s(x)+\bar{s}(x)\right]$$

$$\nu W_2^{en}(x) = \frac{4}{9} x\left[d(x)+\bar{d}(x)\right] + \frac{1}{9} x\left[u(x)+\bar{u}(x)\right] + \frac{1}{9} x\left[s(x)+\bar{s}(x)\right]$$

$$
\begin{aligned}
\nu W_2^{\nu p}(x) &= 2 \times \left[d(x) + \bar{u}(x) \right] \\
\nu W_2^{\bar{\nu} p}(x) &= 2 \times \left[u(x) + \bar{d}(x) \right] \\
\nu W_3^{\nu p}(x) &= 2 \times \left[\bar{u}(x) - d(x) \right] \\
\nu W_3^{\bar{\nu} p}(x) &= 2 \times \left[\bar{d}(x) - u(x) \right]
\end{aligned}
\tag{18}
$$

Therefore, it is possible in principle to extract the individual distributions and fully describe the Drell-Yan process. The same arguments may be applied to the QCD type of analysis as described in Section 2.5. In practice, however, there is not sufficient overlap of the available data on deep inelastic lepton scattering (DIS) in the kinematical region of x and Q^2 covered by the measurements of the lepton pairs spectra.

8.2 Quark Structure Functions:

The procedure most commonly applied[8,11-13,35] in the QCD phenomenology consist of the following steps:

1. Use the DIS data to extract the parton distributions at low Q^2 and in the limited x range where the measurements do overlap sufficiently.

2. Assume the behaviour of these distributions in the x region not covered by experiments.

3. Extrapolate these distributions to large values of Q^2 using the QCD evolution equation.

As an example, one may quote the results of the analysis of Feynman, Field and Fox, [23 24] who used the quark structure functions given in Table I, with smooth transition between small x and large x regime.

TABLE I

	Valence Quarks		Sea Quarks
	large x	small x	
xu(x)	$(1-x)^3$	$\sqrt{x}\,(1-x)^2$	$(1-x)^{10}$
xd(x)	$(1-x)^4$	$\sqrt{x}\,(1-x)^2$	$(1-x)^7$
xs(x)	--	--	$(1-x)^8$

The resulting fit to the $\mu^+\mu^-$ mass spectrum, shown in Figure 25, falls about a factor of two too low, but the data can be fitted well after the adjustment of poorly known sea distributions. [4]

A more direct approach has been taken by the Columbia-Fermilab-Stony Brook group, which used experimental measurements of deep inelastic electron and muon scattering to extract the sea quark structure functions. Assuming the SU(3) symmetry, i.e., $x\bar{u}(x) = x\bar{d}(x) = x\bar{s}(x) = xS(x)$, the formula (3) may be expressed by:

$$\left.\frac{d^2\sigma^{pN}}{dMdy}\right|_{y=0} = \frac{8\pi\alpha^2}{9M^3} \times S(x) \left[\nu W_2^{1p}(x) + \nu W_2^{1N}(x) - \frac{4}{3} \times S(x)\right] . \qquad (19)$$

Solving Equation (19) the CFS group has found $S(x) = (0.54 \pm 0.02) \times (1-x)^{8.5 \pm 0.1}$. The CFS group has also tried to relax the SU(3) requirements using the following parametrization of the quark

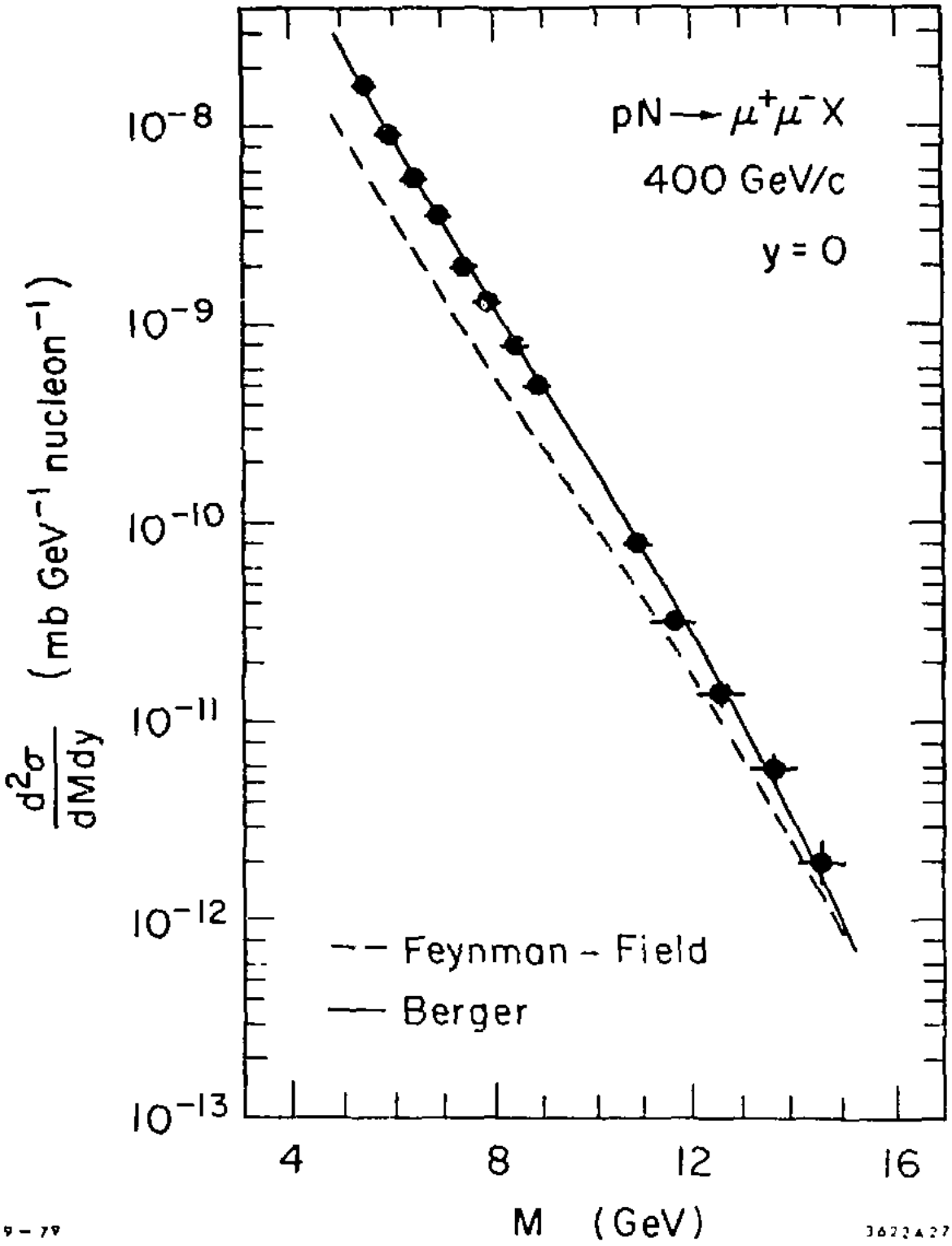

25. QCD fits to the dimuon mass spectrum.

distributions for all Q^2 values:

$$\bar{d}(x) = A(1-x)^n$$

$$\bar{u}(x) = A(1-x)^{n+a}$$

$$\bar{s}(x) = (\bar{u} + \bar{d})/4$$

The results of the fits to the final sample of the data [36] are given in Table II.

TABLE II

	Free Fit	$\bar{u}(x) = \bar{d}(x)$
A	.6[illegible] ± .01	.56 ± .01
n	8.0 ± 0.4	9.0 ± 0.1
a	3.1 ± 0.[illegible]	0
X^2/DF	209/154	291/155

The individual data points for the sea distribution are compared [4] in Figure 26a with those obtained in neutrino interactions by the CERN-Dortmund-Heidelberg-Saclay group. The most striking feature of the graph is the difference, both in shape and in absolute normalization, of the two sets of data. It should be noted, however, that the CDHS data are measured in a rather small Q^2 range with the average value being $Q^2 \sim 15$ GeV^2. On the other hand, the CFS data span rather large range of Q^2 and the scale breaking effects may, therefore, introduce substantial distortion of the shape of the distribution.

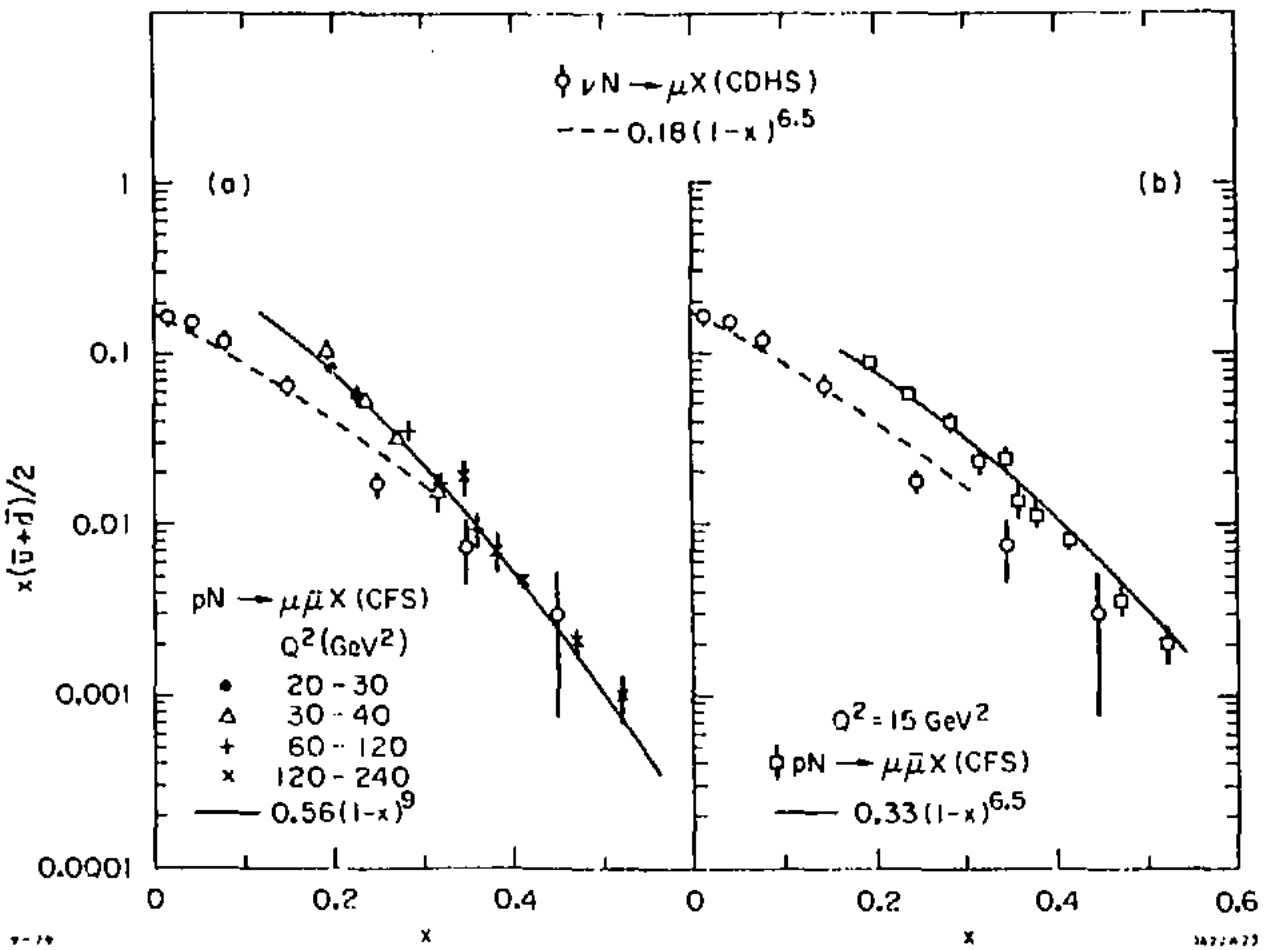

26. Comparison of the proton sea quark distributions measured in neutrino interactions with those obtained from dimuon data:

    a) analysis of Reference 4,

    b) dimuon data "evolved" to $Q^2 = 15\ GeV^2$.

As an example of the size of this effect, the evolution equations as implemented by Abbott and Barnett [37] were used to estimate the values of the CFS points corresponding to $Q^2 = 15\ GeV^2$. The results appeared to be insensitive to the choice of parameterization of the sea distribution; both $(1-x)^{6.5}$ and $(1-x)^9$ dependence resulted in the same (within the errors) changes. The new points shown in Figure 26b have the same x dependence as the CDHS data.

The difference of the normalization of the two sea distributions obtained from the neutrino interactions and from the muon pair production, remains so far an unresolved problem. A possible explanation has been proposed by Altarelli, Ellis and Martinelli, [38] who have calculated in the QCD framework the $O(\alpha_s)$ radiative corrections to the Drell-Yan process. These corrections should be applied when using parton distributions derived from deep inelastic lepton scattering data. The corrections were found to be approximately represented by a scale factor K to the cross sections estimated using prescription given in Section 2.5. In the energy and mass range of existing data, this scale factor K varies slowly between 1.8 and 2. It is at present not clear, whether the radiative corrections will fully explain the normalization discrepancies of the sea distributions. The calculations of Reference 38 were performed for the differential cross section distribution of the lepton pairs and are not directly applicable to the comparison of the sea quark distributions in Figure 26. The size of the $O(\alpha_s)$ correction poses, however, the question of the relative size and sign of higher order terms and their radiative corrections. The complete phonomenological study of the problem has, as yet, not been performed.

8.3 Pion Structure Function:

The measurements of the lepton pairs produced by the pion beam allow for the determination of the pion structure function. For a pion, it follows from charge conjugation and isospin invariance that the x distribution is the same for both valence quarks. Furthermore, in the kinematical region covered by the existing experimental data, it is usually assumed that the contribution to the Drell-Yan process from the pion sea is negligible. In such case, the general form given by Equation (1) reduces to:

$$\frac{d^2\sigma}{dMdx_F} = \frac{8\pi\alpha^2}{9M^2} \frac{1}{(x_1 + x_2)} x_1 \bar{u}^{\pi}(x_1)\left[\frac{4}{9} x_2\, u^N(x_2) + \frac{1}{9} x_2\, \bar{d}^N(x_2)\right] . \qquad (20)$$

The differential cross section distribution expressed in terms of the fractional momenta x_1 and x_2 factorizes into the product of two terms representing the pion and part of the nucleon structure functions:

$$M^2 \frac{d^2\sigma}{dx_1 dx_2} = \frac{4\pi\alpha^2}{9} f^{\pi}(x_1)\, g^N(x_2) \quad , \qquad (21)$$

where $f^{\pi}(x_1) = x_1\, \bar{u}^{\pi}(x_1)$ and $g^N(x_2) = \frac{4}{9} x_2\, u^N(x_2) + \frac{1}{9} x_2\, \bar{d}^N(x_2)$. More generally, without neglecting the pion sea, the Equation (21) may be written as:

$$M^2 \frac{d^2\sigma}{dx_1 dx_2} = \frac{4\pi\alpha^2}{9} \left[f^{\pi}(x_1)\, g^N x_2 + S^{\pi}(x_1)\, h^N(x_2)\right] \quad , \qquad (22)$$

where $S^{\pi}(x_1)$ is the pion sea quark distribution function.

The pion structure function $f^{\pi}(x)$ was obtained[14,15,16] from the measured muon pair data using the above set of equations with the nucleon structure function parametrized following the Buras and Gaemers[33]

analysis of neutrino results. The Chicago-Illinois-Princeton group described the data by

$$f^{\pi}(x) = (.90 \pm .06)\ \sqrt{x}\ (1-x)^{1.27 \pm .06} ,$$

The Saclay-Imperial College-Southampton-Indiana Collaboration used:

$$f^{\pi}(x) = (2.43 \pm .30)\ x(1-x)^{1.57 \pm .18} ,$$

while the CERN-NA3 group obtained good fit with

$$f^{\pi}(x) = (.55\ x)^{-.40 \pm .06}\ (1-x)^{.30 \pm .06}$$

and

$$S^{\pi}(x) = (.09 \pm .06)(1-x)^{4.4 \pm 1.9}$$

The three results are in a disagreement with each other as to the absolute normalization of the results. After the arbitrary normalization of the three $f^{\pi}(x)$, as shown in Figure 27, the data points measured by these experiments coalesce, indicating that the shape of the pion structure function is much flatter than that of the proton. There remains, however, a discrepancy in the resulting nucleon structure function. Part of this discrepancy may be related to the different nuclear target dependence used by various groups (see Section 3.1) and resulting different absolute cross sections for the π induced Drell-Yan process. It is also possible that the QCD corrections suggested in Reference 38 for the proton production has been non-negligible contribution in the case of πN interaction. More detailed study of the nuclear target dependence is expected to resolve this uncertainty.

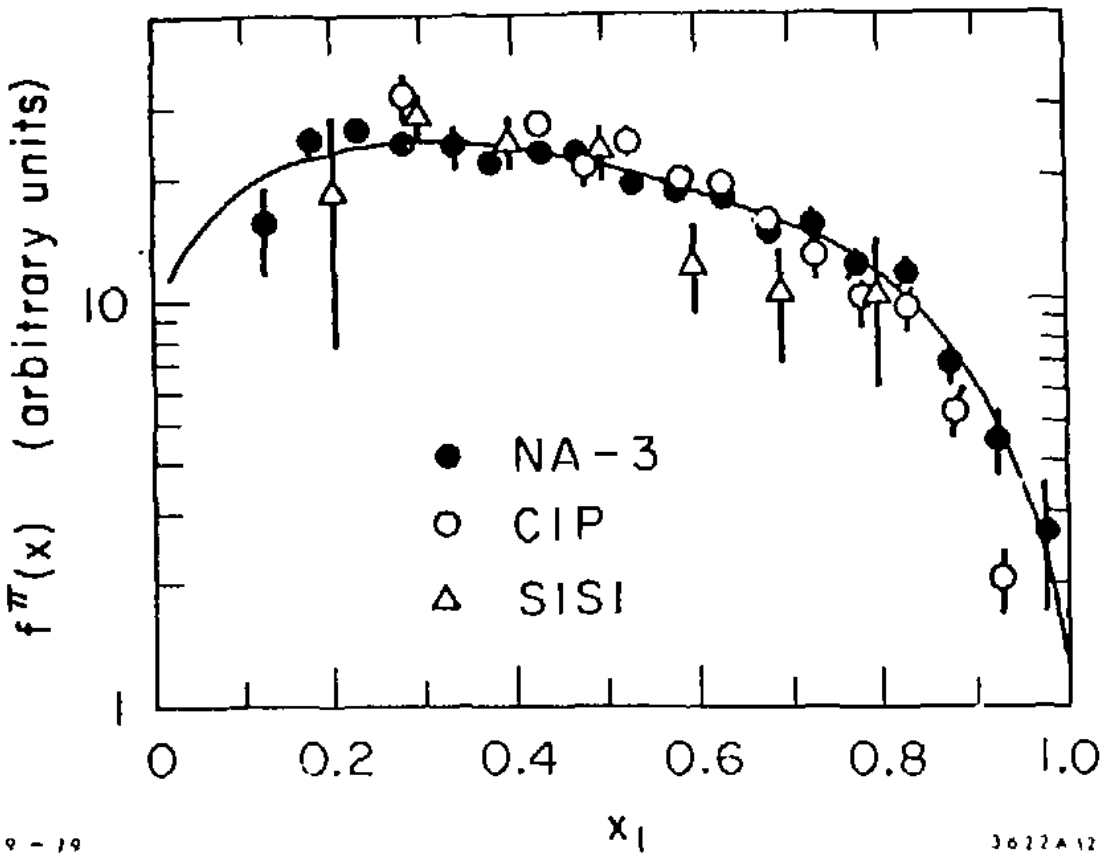

27. Pion structure function.

It should be also remembered that the correct procedure for comparing the structure functions measured in different experiments should include the effects of scale breaking. This is illustrated in Figure 28 where the pion structure function obtained in the low energy experiment[40] is compared with the 225 GeV/c CIP measurements. The results seem to be quite different. The fit to the 22 GeV/c data

$$f^{\pi}(x) = .69\ (1-x)^{.47}$$

was then used as input to the evolution equations. The resulting curve, also shown in Figure 28, gives a good description of the pion structure function at 225 GeV/c.

9 OUTLOOK

The topic of massive lepton pair production plays at present a dual role. On one hand it is one of the most sensitive testing grounds of the QCD phenomenology allowing for the detailed comparison of the theoretical calculations with experimental data. On the other hand, in the framework of the parton model or QCD, it makes possible a study of the structure functions of unstable hadrons like pions, kaons or antiprotons. New experiments performed at CERN and Fermilab will provide accurate results allowing better determination of pion structure function. The question of higher order QCD corrections to the Drell-Yan process will be well studied in the $\bar{p}$ induced muon production. One may expect the coming year to be an exciting one.

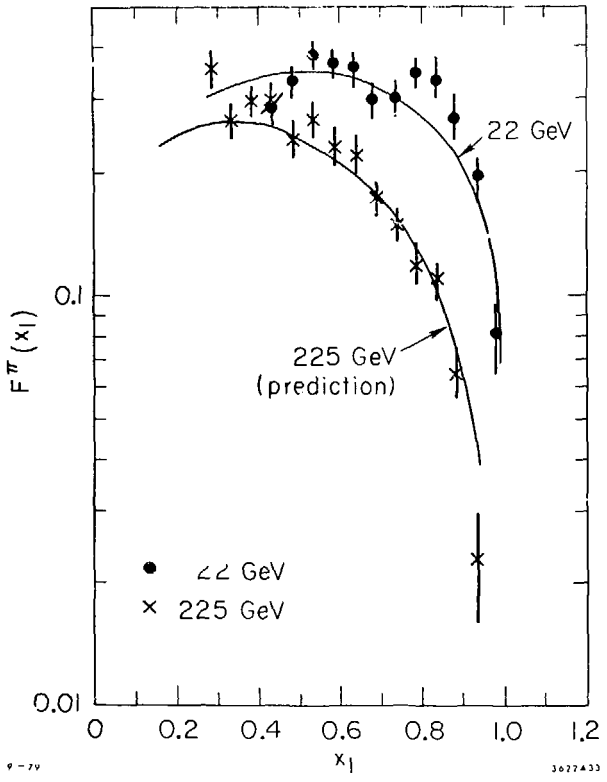

28. Comparison of the pion structure function at 22 GeV/c and 225 GeV/c. The 22 GeV/c were fitted with $f^{\pi}(x) = 0.69\ (1-x)^{.47}$. The curve describing the 225 GeV/c results is the extrapolation of the 22 GeV/c fit using the evolution equation.

ACKNOWLEDGMENTS

In the course of preparing these lectures, I have profited greatly from many conversations with my colleagues at Stanford Linear Accelerator Center. I would like to thank E. L. Berger, S. Brodsky, R. Field and W. Innes for many clarifying discussions.

REFERENCES

1. J. Christenson et al., Phys. Rev. Lett. 25, 1523 (1970) and Phys. Rev. D8, 2016 (1973).

2. S. D. Drell and T. M. Yan, Phys. Rev. Lett. 25, 316 (1970) and Ann. Phys. (N.Y.) 66, 578 (1971).

3. L. M. Lederman, Physics Reports C26, 149 (1976) and Rapporteurs talk at the 19th International Conference on High Energy Physics, Tokyo, 1978.

4. E. L. Berger, Proceedings of the 3rd International Conference at Vanderbilt University on New Results in High Energy Physics and Invited talk at the Orbis Scientiae 1979, Coral Gables, Florida, Stanford Linear Accelerator Center preprint SLAC-PUB-2314.

5. W. E. Caswell, R. R. Horgan and S. J. Brodsky, Phys. Rev. D18, 2415 (1978); R. R. Horgan and P. M. Scharbach, Phys. Lett. 81B, 215 (1979).

6. R. P. Feynman, "Photon-Hadron Interactions" (Benjamin, Reading, Mass., 1972).

7. G. Altarelli, G. Parisi and R. Petronzio, Phys. Lett. 76B, 351 (1978) and Phys. Lett. 76B, 356 (1978).

8. R. D. Field, Invited talk at the 19th International Conference on High Energy Physics, Tokyo, 1978.

9. H. D. Politzer, Nucl. Phys. B129, 301 (1977).

10. C. T. Sachrajda, Phys. Lett. 73B, 185 (1978).

11. K. Kajantie and R. Raitio, Nucl. Phys. B139, 72 (1978).

12. F. Halzen and D. Scott, Phys. Rev. D18, 3378 (1978) and Phys. Rev. D19, 216 (1979).

13. M. Gluck and E. Reya, Nucl. Phys. B130, 76 (1977).

14. K. J. Anderson et al., Phys. Rev. Lett. 42, 944 (1979); G. E. Hogan et al., Phys. Rev. Lett. 42, 948 (1979); C. B. Newman et al., Phys. Rev. Lett. 42, 951 (1979)

15. J. Badier et al., Papers submitted to EPS International Conference on High Energy Physics, Geneva 1979, CERN preprints EP 79-67 EP 79-68.

16. C. Reece et al., "The contribution of $q\bar{q}$ annihilation to dimuon production in πN interactions," University of Rochester report UR-698 (1979).

17. D. C. Hom et al., Phys. Rev. Lett. 37, 1374 (1976); D. M. Kaplan et al., Phys. Rev. Lett. 40, 435 (1978); J. K. Yoh et al., Phys. Rev. Lett. 41, 684 (1978) and Phys. Rev. Lett. 41, 1083 (1978).

18. F. Vanucci, Contribution to the Karlsruhe Summer Institute, Karlsruhe, 1978.

19. Seattle-Northeastern-Michigan-Tufts Collaboration, paper submitted to the 19th International Conference on High Energy Physics, Tokyo, 1978.

20. H. Fritzsch and P. Minkowski, Phys. Lett. 73B, 80 (1978).

21. K. Kajantie, J. Lindfors and R. Raitio, Phys. Lett. 74B, 384 (1978) and Nucl. Phys. B144, 422 (1978).

22. R. D. Field, Lectures at the LaJolla Institute Summer Workshop, 1978, Caltech preprint CALT-68-696.

23. G. C. Fox, Invited talk at the Orbis Scientiae 1978 (Coral Gables), Caltech preprint CALT-68-643.

24. R. P. Feynman, R. D. Field and G. C. Fox, Phys. Rev. D18, 3320 (1978).

25. M. Duong-van, K. V. Vasavada and R. Blankenbecler, Phys. Rev. D16, 1389 (1977); M. Doung-van and R. Blankenbecler, Phys. Rev. D17, 1826 (1977).

26. C. M. Debeau and D. Silverman, Stanford Linear Accelerator Center preprint SLAC-PUB-2187 (1978).

27. S. D. Ellis and R. Stroynowski, Rev. of Mod. Phys. 49, 753 (1977).

28. Yu L. Dokshitser, K. I. Dyakonov and S. I. Troyan, Proceedings of the 13th Leningrad Winter School on Elementary Particle Physics, 1978. SLAC Translations-183.

29. K. Gottfried and J. D. Jackson, Nuovo Cimento 33, 309 (1964).

30. J. C. Collins and D. E. Soper, Phys. Rev. D16, 2219 (1977).

31. K. J. Anderson et al., "Evidence for Longitudinal Polarization in Muon Pair Production by Pions," University of Chicago preprint EFI 79-34.

32. J. Cleymans and M. Kuroda, Phys. Lett. 80B, 385 (1979) and Nucl. Phys. B155, 480 (1979).

33. E. L. Berger and S. J. Brodsky, Phys. Rev. Lett. 42, 940 (1979).

34. F. Gilman, Proceedings of the SLAC Summer Institute on Particle Physics, 1975, M. Zipf, ed., Stanford Linear Accelerator Center SLAC Report No. 191.

35. M. Gluck and E. Reya, Nucl. Phys. B145, 24 (1978).

36. W. Innes, private communication.

37. L. F. Abbott and R. M. Barnett, Stanford Linear Accelerator Center preprint SLAC-PUB-2325 (1979).

38. G. Altarelli, R. K. Ellis and G. Martinelli, Massachusetts Institute of Technology preprint MIT-CTP-776 (1979).

39. A. J. Buras and K. J. F. Gaemers, Nucl. Phys. B132, 249 (1978).

40. D. McCal et al., "Experimental Determination of the Structure Function of the Pion," University of Rochester report UR-699 (1979).